

# Bacterial-fungal interactions revealed by genome-wide analysis of bacterial mutant fitness

Emily C. Pierce<sup>1</sup>, Manon Morin<sup>1</sup>, Jessica C. Little<sup>2</sup>, Roland B. Liu<sup>1</sup>, Joanna Tannous<sup>3</sup>, Nancy P. Keller<sup>3,4,5</sup>, Kit Pogliano<sup>1</sup>, Benjamin E. Wolfe<sup>6</sup>, Laura M. Sanchez<sup>2</sup> and Rachel J. Dutton<sup>1,7</sup>

Microbial interactions are expected to be major determinants of microbiome structure and function. Although fungi are found in diverse microbiomes, their interactions with bacteria remain largely uncharacterized. In this work, we characterize interactions in 16 different bacterial-fungal pairs, examining the impacts of 8 different fungi isolated from cheese rind microbiomes on 2 bacteria (*Escherichia coli* and a cheese-isolated *Pseudomonas psychrophila*). Using random barcode transposon-site sequencing with an analysis pipeline that allows statistical comparisons between different conditions, we observed that fungal partners caused widespread changes in the fitness of bacterial mutants compared to growth alone. We found that all fungal species modulated the availability of iron and biotin to bacterial species, which suggests that these may be conserved drivers of bacterial-fungal interactions. Species-specific interactions were also uncovered, a subset of which suggested fungal antibiotic production. Changes in both conserved and species-specific interactions resulted from the deletion of a global regulator of fungal specialized metabolite production. This work highlights the potential for broad impacts of fungi on bacterial species within microbiomes.

espite growing awareness that fungi have an immense capacity to affect ecosystems, fungi are frequently overlooked in microbiome studies<sup>1,2</sup>. Recently, fungi and other microeukaryotes have received increased attention in sequencing-based studies<sup>3-6</sup>, and there is growing interest in exploring the roles that fungi and bacterial-fungal interactions play in environmental and host-associated microbiomes<sup>7-10</sup>. While specific interaction mechanisms have been elucidated for pairwise bacterial-fungal associations, including important pathogenic bacteria and fungi<sup>11-14</sup>, analysing a greater diversity of bacterial-fungal interactions could lead to a better ability to predict when and how these interactions contribute to microbiome diversity and function. However, a broader characterization of bacterial-fungal interactions has been challenging given the complexity of many microbiomes.

Cheese rind biofilms have been developed as experimentally tractable systems to study microbiomes. These multi-kingdom biofilms form on the surface of cheese during the ageing process. Prior work using this system has demonstrated that fungi can affect bacterial growth<sup>15</sup>. For example, fungi were shown to cross-feed amino acids to bacteria when grown on a cheese-based medium<sup>16</sup>. Fungal hyphal networks can also alter the composition of a rind microbiome community by providing a means of dispersal for certain community members<sup>17</sup>.

Here, we combined the high-throughput genetic screening method random barcode transposon-site sequencing (RB-TnSeq)<sup>18</sup> with RNA sequencing (RNA-seq), bacterial cytological profiling and metabolomics to investigate bacterial–fungal interactions. Building on existing tools, we created a customized computational RB-TnSeq<sup>18</sup> pipeline that enabled us to specifically examine the differences in bacterial growth alone versus in the presence of a fungal partner to highlight pathways that are important during interactions. We examined

pairwise combinations of eight fungal species isolated from cheese rinds (two yeasts and six filamentous fungi) and two bacteria, *Pseudomonas psychrophila* strain (str.) JB418 and *Escherichia coli* K12.

We observed broad changes in bacterial mutant fitness in the presence of fungi compared to growth alone. A consistent impact across fungal species was the alleviation of the requirement by E. coli for its own siderophore, enterobactin. Further genetic analysis suggested that this alleviation is due to the uptake of siderophores produced by filamentous fungi. We observed similar alleviation when E. coli was grown with soil and skin fungi, which suggests that fungal siderophores may affect bacterial growth in other systems. In addition, we found evidence to indicate that fungi increase the need for biotin biosynthesis in both E. coli and P. psychrophila. Furthermore, multiple lines of evidence suggested that several filamentous fungal species produce antimicrobials. Deletion of laeA, a gene encoding a global regulator of fungal specialized metabolite production, led to a large decrease in the number of affected pathways in bacteria, which suggests that specialized metabolites play an important role in bacterial-fungal interactions.

#### Results

Characterization of bacterial genes with differential fitness in the presence of fungal partners. We selected a panel of eight fungi commonly found in cheese rind microbiomes, all of which belong to the phylum Ascomycota (Fig. 1). They include two yeasts, *Candida* sp. str. 135E and *Debaryomyces* sp. str. 135B, and six filamentous fungi, *Penicillium* sp. str. 12, *Penicillium* sp. str. SAM3, *Penicillium* sp. str. RS17, *Fusarium* sp. str. 554A, *Scopulariopsis* sp. str. JB370 and *Scopulariopsis* sp. str. 165-5. These genera are also found in the human gut mycobiomes<sup>19</sup>, in soil microbiomes<sup>20</sup>, in other agricultural microbiomes<sup>21</sup> and in marine environments<sup>22</sup>.

<sup>1</sup>Division of Biological Sciences, University of California, San Diego, La Jolla, CA, USA. <sup>2</sup>Department of Pharmaceutical Sciences, College of Pharmacy, University of Illinois at Chicago, Chicago, IL, USA. <sup>3</sup>Department of Medical Microbiology and Immunology, University of Wisconsin-Madison, Madison, WI, USA. <sup>4</sup>Department of Bacteriology, University of Wisconsin-Madison, Madison, WI, USA. <sup>5</sup>Food Research Institute, University of Wisconsin-Madison, Madison, WI, USA. <sup>6</sup>Department of Biology, Tufts University, Medford, MA, USA. <sup>7</sup>Center for Microbiome Innovation, Jacobs School of Engineering, University of California, San Diego, La Jolla, CA, USA. <sup>⊠</sup>e-mail: rjdutton@ucsd.edu

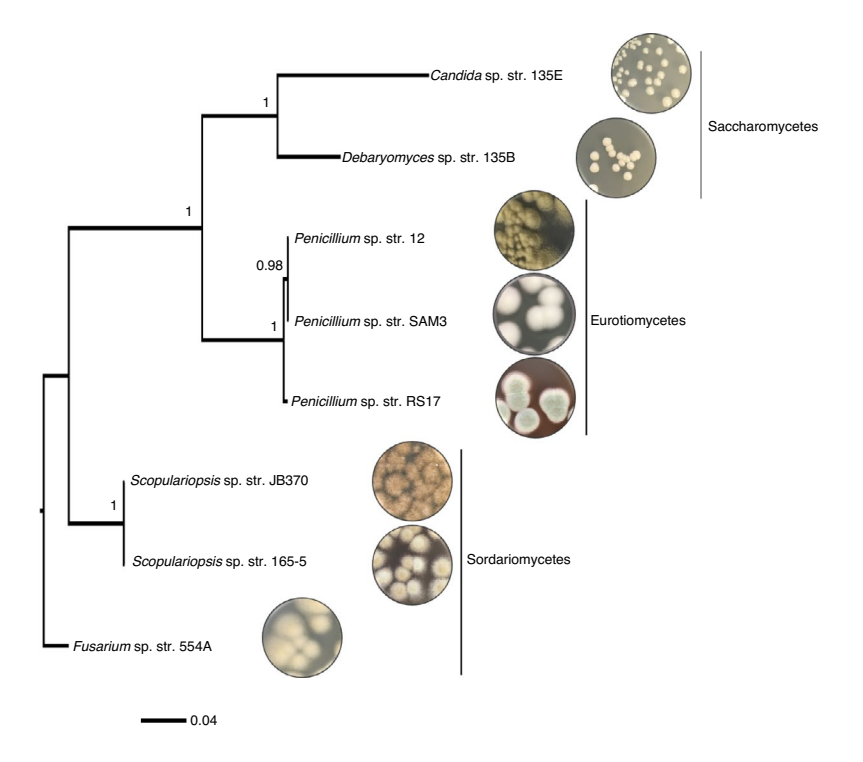


**Fig. 1| Fungal interaction partners span the phylogenetic and morphological diversity of the cheese ecosystem.** A phylogenetic tree based on the large subunit ribosomal RNA of the cheese fungi used as interaction partners in this study. The tree was built using Bayesian phylogenetic inference with MrBayes<sup>58</sup> and the Jukes and Cantor substitution model<sup>98</sup>. Branch labels display posterior probability values.

The selected bacterial interaction partners were two species of Gammaproteobacteria, *P. psychrophila* str. JB418 and *E. coli* K12 BW25113. Proteobacteria are common inhabitants of cheese rind communities and are responsive to the presence of fungi in experimental community conditions<sup>15</sup> (Supplementary Figs. 1 and 2). *P. psychrophila* str. JB418 was originally isolated from a cheese rind. *E. coli* K12 was selected as a bacterial partner to take advantage of the genetic resources available for this organism. Furthermore, *E. coli* can be a causative agent of foodborne illness in cheese and other foods<sup>23,24</sup>.

Using a pooled library of barcoded transposon-insertion mutants, RB-TnSeq18 generates a fitness value for each gene that reflects the importance of a gene for survival in the experimental condition. A negative fitness value indicates that disruption of a given gene leads to decreased growth relative to a wild-type (WT) strain, whereas a positive value indicates enhanced growth, with values further from 0 indicating stronger effects of gene disruption. To identify bacterial mutants with a significantly different fitness value in the presence of a fungal partner compared to growth alone, pooled P. psychrophila<sup>16</sup> or E. coli<sup>18</sup> RB-TnSeq mutant libraries were grown for 7 days on solid cheese curd agar (CCA) plates<sup>25</sup> either alone or mixed with one of the eight fungal species. As sporulation is associated with production of many fungal specialized metabolites, we selected the 7-day time point to capture interactions related to these metabolites<sup>26</sup>. A custom computational pipeline allowed us to quantitatively compare fitness values between conditions (Extended Data Fig. 1 and Supplementary Method 1; https://github. com/DuttonLab/RB-TnSeq-Microbial-interactions). The difference between these fitness values is hereafter referred to as 'interaction fitness' (Fig. 2 and Extended Data Fig. 2). In some cases, the presence of a fungus increased the fitness of a mutant (positive interaction fitness), whereas in others, the fitness of a mutant decreased (negative interaction fitness) (Supplementary Tables 1 and 2).

In total, we found 731 *E. coli* and 1,606 *P. psychrophila* genes whose disruption led to a change in fitness in the presence of at

least one of the fungal partners (Supplementary Tables 3 and 4). This represents an average of  $216 \pm 50$  *E. coli* genes per fungal condition and  $576 \pm 122$  *P. psychrophila* genes per fungal condition that have an interaction fitness. For *E. coli*, interaction fitness values ranged from -5.66 to 5.71, and for *P. psychrophila*, -6.18 to 5.74, which highlights the large positive and negative impacts of fungion bacteria.

To assess the degree of conservation of these fitness effects, we identified homologous genes between *E. coli* and *P. psychrophila* (Supplementary Tables 5 and 6 and Extended Data Fig. 3). The set of 88 genes with interaction fitness for both *E. coli* and *P. psychrophila* in the same set of fungal conditions was enriched for genes in amino acid biosynthesis, including isoleucine/valine biosynthesis. The isoleucine/valine biosynthesis genes have a negative interaction fitness with both bacteria, which suggests that fungi may be competing for amino acids available from cheese (Supplementary Table 7). We have previously seen 16 that these genes are important for *E. coli* growth alone on cheese, which suggests that these amino acids may be limited in this medium.

To assess the specificity of fungal impacts on bacteria, we evaluated the intersections of gene sets across the entire set of fungal interaction conditions (Fig. 3a, Extended Data Fig. 4 and Supplementary Tables 8 and 9). Around 21% (n=152) of the interaction-related genes for E. coli and 32% (n=508) for P. psychrophila were common to at least four out of the eight fungal interaction conditions (Fig. 3b). In addition to conserved effects, we observed a large number of fungal species-specific effects. For E. coli, 45% of the genes with interaction fitness were specific to a single fungus (n=329), whereas for P. psychrophila, it was 37% (n = 599). For both E. coli and P. psychrophila, growth with Penicillium sp. str. 12 and Penicillium sp. str. SAM3 resulted in a large number of the same genes with significant interaction fitness (n=83 and n=318, respectively; Fig. 3b). These species also clustered away from the other fungi in a principal component analysis (Extended Data Fig. 5).

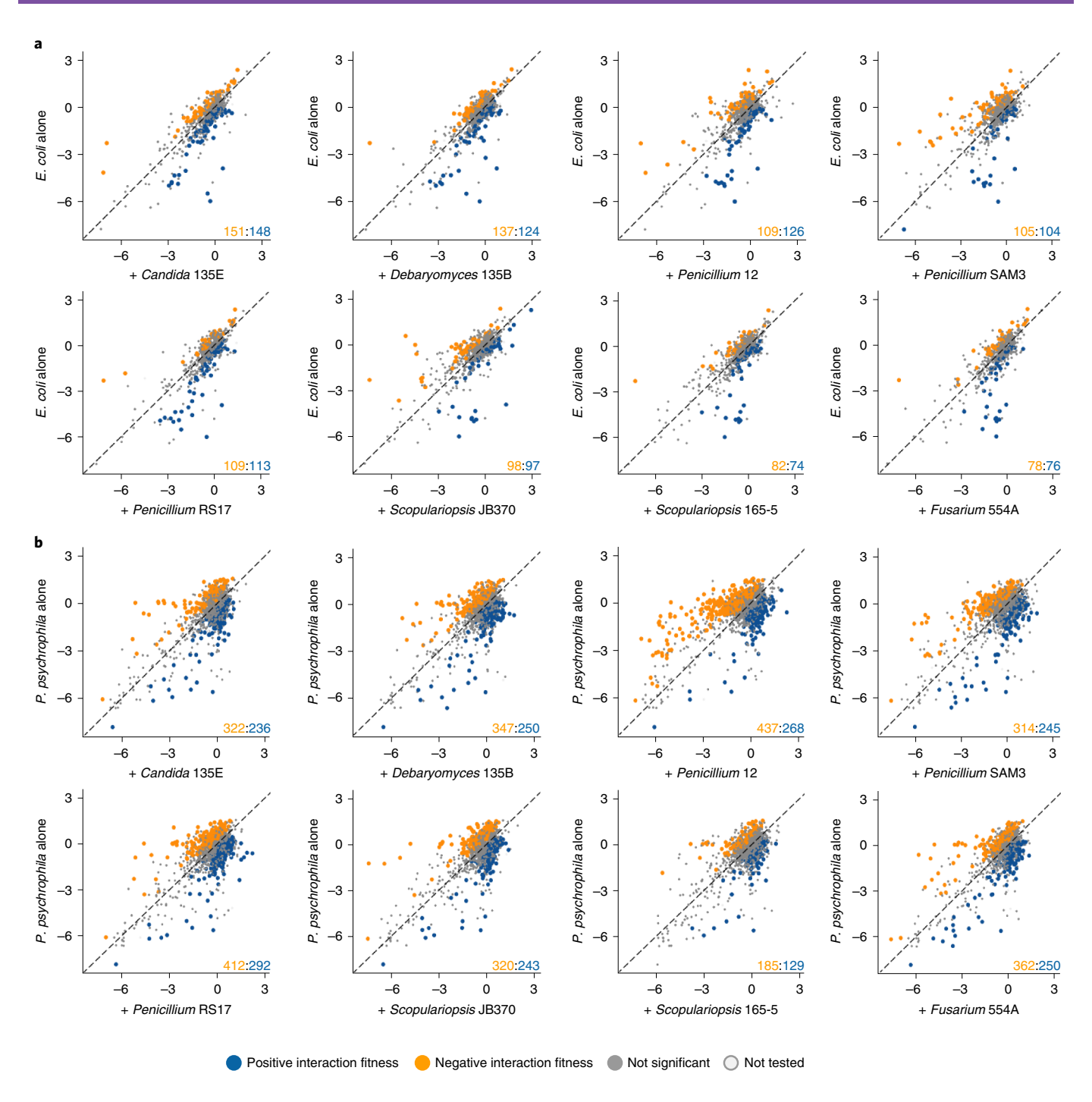


**Fig. 2 | Comparison of bacterial gene fitness with fungi against growth alone and identification of bacterial genes with significant interaction fitness across fungal partners. a,b,** Gene fitness values for *E. coli* (a) and *P. psychrophila* (b) were calculated for each gene during growth with a fungal partner (x axis) and during growth alone (y axis). Each point represents a gene, with coloured points indicating genes with a significant difference between gene fitness during growth alone versus with a fungal partner identified by a two-sided t-test and an adjusted P value lower than 5% using Benjamini-Hochberg correction for multiple comparison testing. This difference is hereafter referred to as 'interaction fitness'. Exact P values are provided in Supplementary Tables 1 and 2. The coloured numbers in the lower right-hand corner indicate how many genes have either positive (blue) or negative (orange) interaction fitness. Positive interaction fitness indicates that a gene fitness value is significantly higher in the presence of the fungal partner compared to growth alone while negative interaction fitness indicates a lower fitness value in the presence of the fungal partner. Nonsignificant points are plotted smaller to aid in the visualization of significant genes. Genes not included in the t-test are labelled as not tested.

**Penicillium** sp. str. 12 and **Penicillium** sp. str. SAM3 induce bacterial envelope stress. We used the following combination of methods to identify potential mechanisms underlying bacterial-fungal interactions: categorization of clusters of orthologous genes (COG), analysis of functional enrichment and analysis of the

conservation of the effect across fungal species (Fig. 3c, Supplementary Tables 10 and 11 and Extended Data Fig. 6). *Penicillium* sp. str. 12 and *Penicillium* sp. str. SAM3 consistently shared effects on bacterial mutant fitness, as seen by their large number of network connections (Fig. 3a). The gene sets affected

by these fungi suggest that these two fungal species are creating bacterial envelope stress, potentially through the production of antibiotic molecules, as they include drug efflux pumps, envelope stress response systems, penicillin-binding proteins and lipopoly-saccharide/peptidoglycan biosynthesis genes (Supplementary Table 12). For example, disruption of the multidrug efflux pump MdtK resulted in a decreased fitness specifically in the presence of these two fungi (gene fitness alone = 0.34, with *Penicillium* sp. str. 12 = -2.49, with *Penicillium* sp. str. SAM3 = -1.92).

We performed bacterial cytological profiling (BCP) $^{27}$ , a microscopy-based method used to predict the mechanism of action for antibiotics, on WT or  $\Delta mdtK$  *E. coli* grown alone or in a mixed biofilm with *Penicillium* sp. str. 12 or *Penicillium* sp. str. SAM3. Microscopy analysis showed a strong change in cell morphology for both WT and  $\Delta mdtK$  *E. coli* when grown with *Penicillium* compared to growth alone (Fig. 4a). When cultured with these fungi, *E. coli* cells were significantly more round, which is consistent with a reduction in cell wall integrity (Fig. 4b).  $\Delta mdtK$  cells were strongly affected and were spheroplasted, which is indicative of the complete loss of structural integrity. Control experiments with known antibiotic compounds showed that this effect is similar to that of antibiotics that target cell wall biosynthesis, such as mecillinam and amoxicillin (Fig. 4 and Extended Data Fig. 7).

Previous studies have shown that fungal specialized metabolite production in other ascomycete fungi is controlled by the global regulator LaeA  $^{28,29}$ . To test the contribution of this gene to the potential antibiotic activity observed, we generated a  $\Delta laeA$  mutant in Penicillium sp. str. 12. WT  $E.\ coli$  cells were significantly less round when grown with Penicillium sp. str. 12  $\Delta laeA$ , which suggests that loss of this global regulator has potentially decreased fungal antibiotic production (Fig. 4). Neither of these two fungal strains are known producers of penicillin, and an analysis of the Penicillium sp. str. 12 draft genome failed to detect penicillin biosynthesis gene clusters  $^{30}$ . However, both fungi were causing consistent morphological and genetic effects that suggest that these fungi induce cell envelope stress similar to that seen with  $\beta$ -lactam antibiotics.

Fungi increase the bacterial need for biotin biosynthesis. *P. psychrophila* RB-TnSeq data showed that the disruption of genes associated with biotin biosynthesis (*bioB*, *bioD*, *bioF*, *bioA*, *bioH* and *bioC*) results in a negative interaction fitness with most fungi (average fitness alone=0.08, average fitness across fungi=-2.97) (Fig. 3c). This gene set represents all genes needed to synthesize biotin from pimeloyl-CoA. Biotin is present in our CCA medium at 73 nmol mg<sup>-1</sup> and represents an essential cofactor for enzymes involved in key cellular functions such as amino acid metabolism and lipid synthesis<sup>31</sup>. In *E. coli*, biotin biosynthesis genes exhibited a neutral fitness alone and did not show interaction fitness in our RB-TnSeq experiments. However, RNA-seq of WT *E. coli* grown

either alone or in the presence of *Penicillium* sp. str. 12, a predicted biotin prototroph, showed that *bioA*, *bioB*, *bioC*, *bioD* and *bioF* were all significantly upregulated in the presence of *Penicillium* sp. str. 12, with an average fold change of 4.4 (Supplementary Table 13). This highlights an increased need for bacterial biotin synthesis in both *P. psychrophila* and *E. coli*, which suggests that there is competition for available biotin in the medium or that bacteria have higher biotin requirements in the presence of these fungi.

Fungi increase iron availability for bacterial partners. Because cheese is an iron-limited environment (with free iron levels of approximately  $3 \text{ ppm}^{32}$ ), microbial species require iron chelators such as siderophores to  $\text{grow}^{16,32,33}$ . Our RB-TnSeq fitness data revealed that *E. coli* mutants that are defective in the transport of its siderophore, enterobactin, grow poorly in the alone condition (fitness < -4). However, the presence of any fungal partner significantly improved the growth of mutants in the *fep* operon (*fepC*, *fepG*, *fepA* and *fepB*), which encodes enterobactin transport functions (average positive interaction fitness of 3.11) (Fig. 3c, Fig. 5a and Supplementary Table 10). The positive effect of fungi on growth was further supported by competitive mutant fitness assays with isolated enterobactin uptake mutants (Fig. 5b).

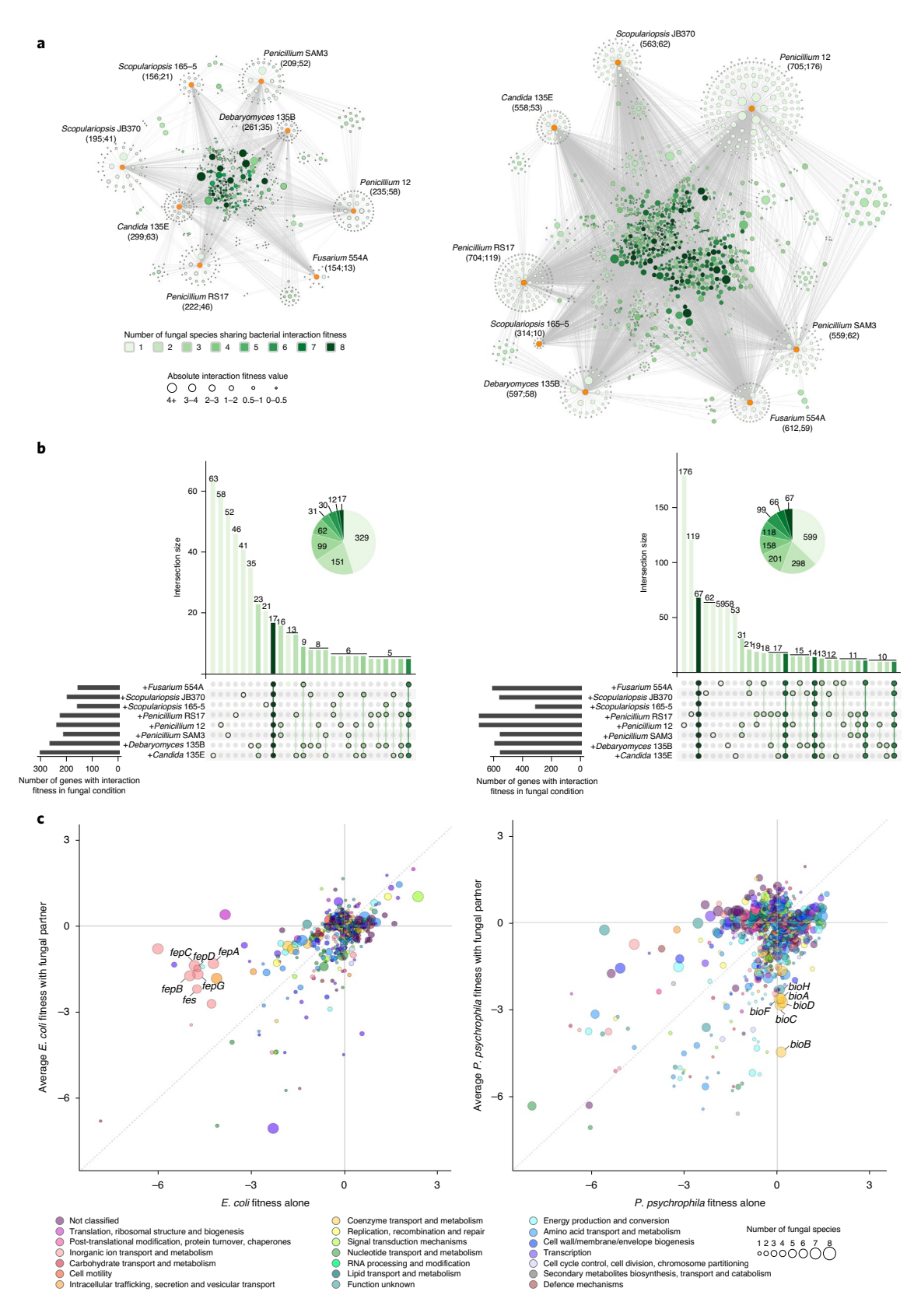
Although siderophore production and uptake have not been previously characterized in *P. psychrophila* str. JB418, three putative iron-related genes have an effect similar to that seen with *E. coli fep* genes (having a fitness defect alone, but a positive interaction fitness with any fungus): Ga0212129\_113525, Ga0212129\_115698 and Ga0212129\_114260. These genes are annotated as iron-complex outer membrane receptor protein, as putative iron-dependent peroxidase and as uncharacterized iron-regulated membrane protein, respectively. Immediately upstream of Ga0212129\_114260, we found a ferric enterobactin receptor (FepA) and the PfeR–PfeS two-component regulatory system required for the ferric enterobactin receptor<sup>34</sup>. Although pyochelin and pyoverdine are two well-known *Pseudomonas* siderophores<sup>35</sup>, antiSMASH did not predict these siderophores in *P. psychrophila*.

RNA-seq analysis of WT *E. coli* revealed 34 genes (out of a total of 348 significantly upregulated genes) involved in iron acquisition that were specifically upregulated in the presence of *Penicillium* sp. str. 12 (Supplementary Table 14). We observed upregulation of enterobactin biosynthesis and uptake (*ent-* and *fep-*associated genes), which suggests that even in the presence of fungi, *E. coli* still produces and utilizes its native siderophore (Fig. 5c). In addition to the enterobactin uptake system, *E. coli* possesses the Fhu system, which enables the uptake of hydroxamate-type siderophores, including those produced by fungi, such as ferrichrome and coprogen<sup>36,37</sup>. Notably, our RNA-seq data showed upregulation of *fhuA* (which encodes an outer membrane receptor for ferrichrome)

**Fig. 3 | Cross-comparison and functional characterization of bacterial genes with interaction fitness in the presence of fungi. a**, Network of *E. coli* (left) or *P. psychrophila* (right) genes with an interaction fitness based on RB-TnSeq. Each orange node represents a fungal partner and is labelled as follows: fungal partner (number of genes with interaction fitness; number of genes with interaction fitness unique to this condition). Each green node represents a bacterial gene. Green nodes are shaded by the number of fungal conditions in which this gene has an interaction fitness, as shown in the legend below, and are sized by the average strength of interaction fitness across partners. **b**, UpSet<sup>99</sup> plots showing the intersections of *E. coli* (left) or *P. psychrophila* (right) gene sets with interaction fitness across fungal partners. These UpSet plots are conceptually similar to Venn diagrams. The connected circles indicate which fungal conditions are included in the intersection, and the size of the intersection (the number of genes that have an interaction fitness in all the highlighted conditions) is displayed in the main bar chart. The horizontal bar chart displays the number of genes with significant interaction fitness per fungal condition. Intersections with fewer than five genes are not shown for *E. coli* and fewer than ten genes are not shown for *P. psychrophila*. For example, in the *E. coli* panel, 17 genes have an interaction fitness with all partners (all fungi circles are connected), while 16 other genes have an interaction fitness with *Penicillium* sp. str. 12 and with *Penicillium* sp. str. SAM3 (only *Penicillium* sp. str. 12 and *Penicillium* sp. str. SAM3 circles are connected). Intersections are green colour-coded based on the number of fungal partners sharing the interaction as in Fig. 3a. **c**, Comparison of *E. coli* (left) or *P. psychrophila* (right) gene fitness values alone compared to fitness values with a fungal partner, coloured by COG category and sized by the conservat

and *fhuE* (which encodes an outer membrane receptor for coprogen) in the presence of *Penicillium*, which suggests that this fungus may alleviate the growth defects seen in the *fep* mutants through the provision of hydroxamate-type siderophores taken up by the Fhu system.

All filamentous fungi in this study, but not yeast, produce siderophores detectable by the chrome azurol S (CAS) assay (Extended Data Fig. 8). In addition, liquid chromatography—mass spectrometry (LC–MS and LC–MS/MS) showed evidence of the hydroxamate fungal siderophores coprogen and ferrichrome in *Fusarium* 



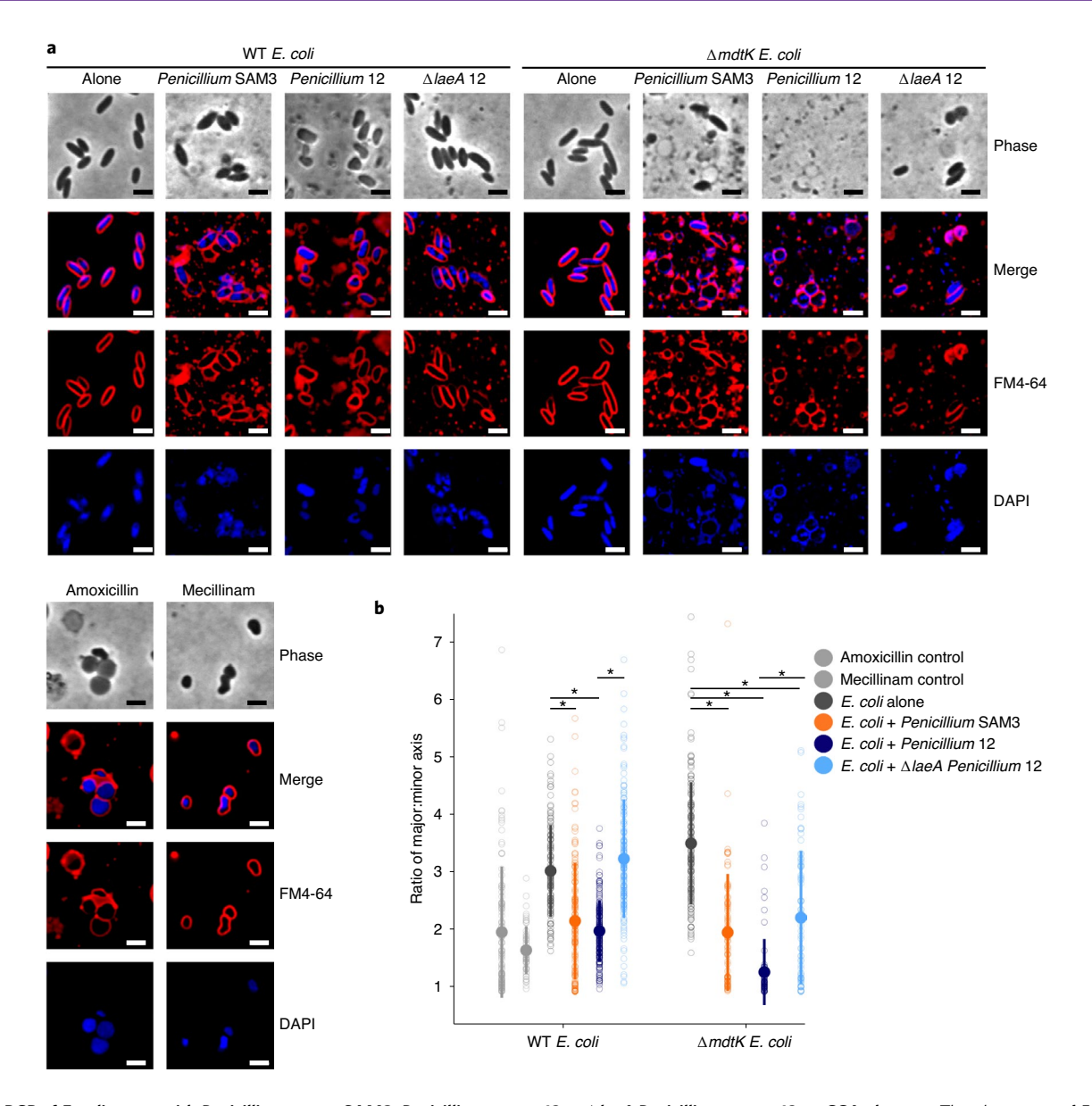


**Fig. 4 | BCP of** *E. coli* grown with *Penicillium* sp. str. SAM3, *Penicillium* sp. str. 12 or  $\Delta$ *laeA Penicillium* sp. str. 12 on CCA plates. a, The phenotype of *E. coli* grown with these fungi is similar to that seen when *E. coli* is exposed to antibiotics targeting cell wall biosynthesis. This effect is more dramatic in *E. coli* lacking the *mdtK* multidrug efflux pump. Representative fields of deconvoluted images are displayed. DAPI dye stains DNA and FM4-64 dye stains bacterial membranes. Scale bars, 2 μm. **b**, Quantification of microscopy results. The major and minor axes of individual cells were measured (all cells in the image for multiple images), and the ratio of these measurements was used as an indicator of cell roundness. Each empty circle represents an individual cell (from left to right, n = 110, 53, 121, 136, 181, 144, 153, 79, 70 and 73 cells examined from one independent experiment per condition). The filled circle displays the mean, and the thick bar extending from the mean displays the standard deviation. WT *E. coli* has a ratio of about 3, and the cells become rounder as the ratio approaches 1. Asterisks indicate significantly different roundness in the presence of a fungus relative to growth alone or significantly different roundness in the presence of WT *Penicillium* sp. str. 12 relative to Δ*laeA Penicillium* sp. str. 12 (unpaired two-sample Wilcoxon test P < 0.05). Exact P values are as follows: E. *coli-Penicillium* SAM3 versus E. *coli-Penicillium* 12 versus E. *coli-Denicillium* 12 versus E.

and *Penicillium* species (Fig. 5d). Although not detected in these extracts, *Scopulariopsis* sp. str. JB370 is predicted to make dimethylcoprogen based on an antiSMASH analysis of the draft genome<sup>38</sup>.

To confirm that hydroxamate siderophores could rescue fep mutants via the Fhu pathway, we verified that purified coprogen and ferrichrome rescued the growth defect of  $\Delta fepA$  or  $\Delta fepC$  mutants grown on CCA (Fig. 5e). As expected, fhuA or fhuE mutants alone did not show a growth defect on CCA, probably because the enterobactin system is intact. Thus, to specifically

examine whether these genes are required for the uptake of the purified siderophores, we constructed *fhuA* or *fhuE* mutants in an enterobactin-uptake-defective background ( $\Delta fepC$  or  $\Delta fepA$ ). The combined loss of enterobactin uptake and *fhuA* eliminated the alleviation seen with ferrichrome, whereas loss of either *fhuA* or *fhuE* in the  $\Delta fepA$  background seemed to eliminate the alleviation seen with coprogen (Fig. 5e). This suggests that *E. coli* requires *fhuA* for ferrichrome uptake, and both *fhuA* and *fhuE* for coprogen uptake.

We next examined whether the presence of fungal species changed the growth of strains defective in siderophore uptake (Fig. 5f and Extended Data Fig. 9). Growth of the  $\Delta fepA$  and  $\Delta fepC$  mutants was restored closest to the filamentous fungi, but not when grown near yeasts. For filamentous fungi, this effect was dependent on either fhuA or fhuE. Thus, E. coli is likely to use and benefit from fungal hydroxamate siderophores produced by filamentous fungi that are taken up by the Fhu system independently of the enterobactin uptake system.

Because iron limitation is a common challenge across many environments, we wanted to examine whether fungal species from other ecosystems could also be producing siderophores that are accessible to neighbouring bacterial species. We performed similar assays with Aspergillus fumigatus, a soil-dwelling filamentous ascomycete, and Malassezia pachydermatis, a basidiomycete yeast that is a commensal resident on animal skin. Our results suggested that A. fumigatus produces a siderophore capable of being imported through FhuA (Fig. 5f). We saw a similar effect using M. pachydermatis, which suggests that bacteria are able to utilize siderophores from a yeast species using the Fhu system (Fig. 5f). We performed an antiSMASH38 analysis on a previously published genome of this M. pachydermatis strain and were able to identify a nonribosomal peptide synthetase (NRPS) biosynthetic gene cluster containing a ferrichrome peptide synthetase<sup>38,39</sup>. In summary, our results suggest that cheese-associated filamentous fungi, and select fungi from other environments, can reduce bacterial dependence on their own siderophores.

Loss of a fungal secondary metabolite regulator alters the profile of interaction fitness. The cases above show that bacterial gene fitness is affected by the production of fungal specialized metabolites, including siderophores and potentially antibiotics. To determine the extent to which the global regulator LaeA is responsible for fungal-induced changes in bacterial fitness, we performed RB-TnSeq experiments with the *Penicillium* sp. str. 12  $\Delta laeA$  mutant. Despite comparable fungal growth between WT and  $\Delta laeA$ , we saw only 65 *E. coli* genes with interaction fitness when grown with  $\Delta laeA$  compared with 204 with WT, which suggests that many of the fitness effects we saw may be due to fungal specialized metabolite production (Fig. 6a and Extended Data Fig. 10).

Given that siderophore production in other fungi is controlled by LaeA, we would expect that  $E.\ coli$  enterobactin uptake mutants would not have positive interaction fitness with the  $\Delta laeA$  mutant. Indeed, we no longer saw a positive interaction fitness for fes, fepA, fepB, fepC, fepD and fepG genes when  $E.\ coli$  was grown with  $\Delta laeA$  Penicillium sp. str. 12 (Supplementary Table 15). Additionally, we saw a negative interaction fitness for the hydroxamate siderophore

transport genes fhuB and fhuC with WT Penicillium sp. str. 12 but not with  $\Delta laeA$ . Liquid CAS assays demonstrated that  $\Delta laeA$  Penicillium sp. str. 12 produced fewer siderophores than WT on cheese medium (Fig. 6b). Overall, these results demonstrate that loss of the LaeA regulator decreases siderophore production in Penicillium sp. str. 12 and abolishes the positive interaction effect seen for fep genes grown with WT fungus.

We next examined whether there were changes in the fitness of genes related to responses to antibiotics. A number of genes involved in cell envelope maintenance showed a negative interaction fitness with WT but not  $\Delta laeA$  Penicillium sp. str. 12 (Supplementary Table 12). These genes included dacA, which encodes penicillin-binding protein 5. Loss of this gene can increase the susceptibility of *E. coli* to  $\beta$ -lactam antibiotics<sup>40</sup>. Mutants in the gene encoding the MdtK efflux protein had improved fitness with  $\Delta laeA$  relative to WT Penicillium sp. str. 12. As seen in our BCP analysis, maintenance of cell envelope integrity is important for *E. coli* growing with WT Penicillium sp. str. 12, but less so in the absence of LaeA.

RNA-seq results showed that 14% of the *Penicillium* sp. str. 12 genome was differentially expressed between WT and  $\Delta laeA$  (Fig. 6c and Supplementary Table 16). This is consistent with previous findings in *A. fumigatus* that LaeA influenced the expression of around 10% of the fungal genome<sup>41</sup>. Gene Ontology (GO) term enrichment analysis identified a number of specialized metabolite biosynthesis pathways overrepresented in the genes that were more expressed in the WT strain (Supplementary Table 17). Of the biosynthetic gene clusters predicted by the antiSMASH<sup>38</sup> analysis, 11 were downregulated in  $\Delta laeA$ , including 1 terpene cluster, 2 type I polyketide synthase clusters and 8 NRPS clusters. Consistent with our findings of decreased siderophore production in  $\Delta laeA$ , one NRPS cluster contained four genes with homology to sidD, sidF, sidH and sitT; these genes are associated with siderophore biosynthesis and transport in  $Aspergillus^{42}$ .

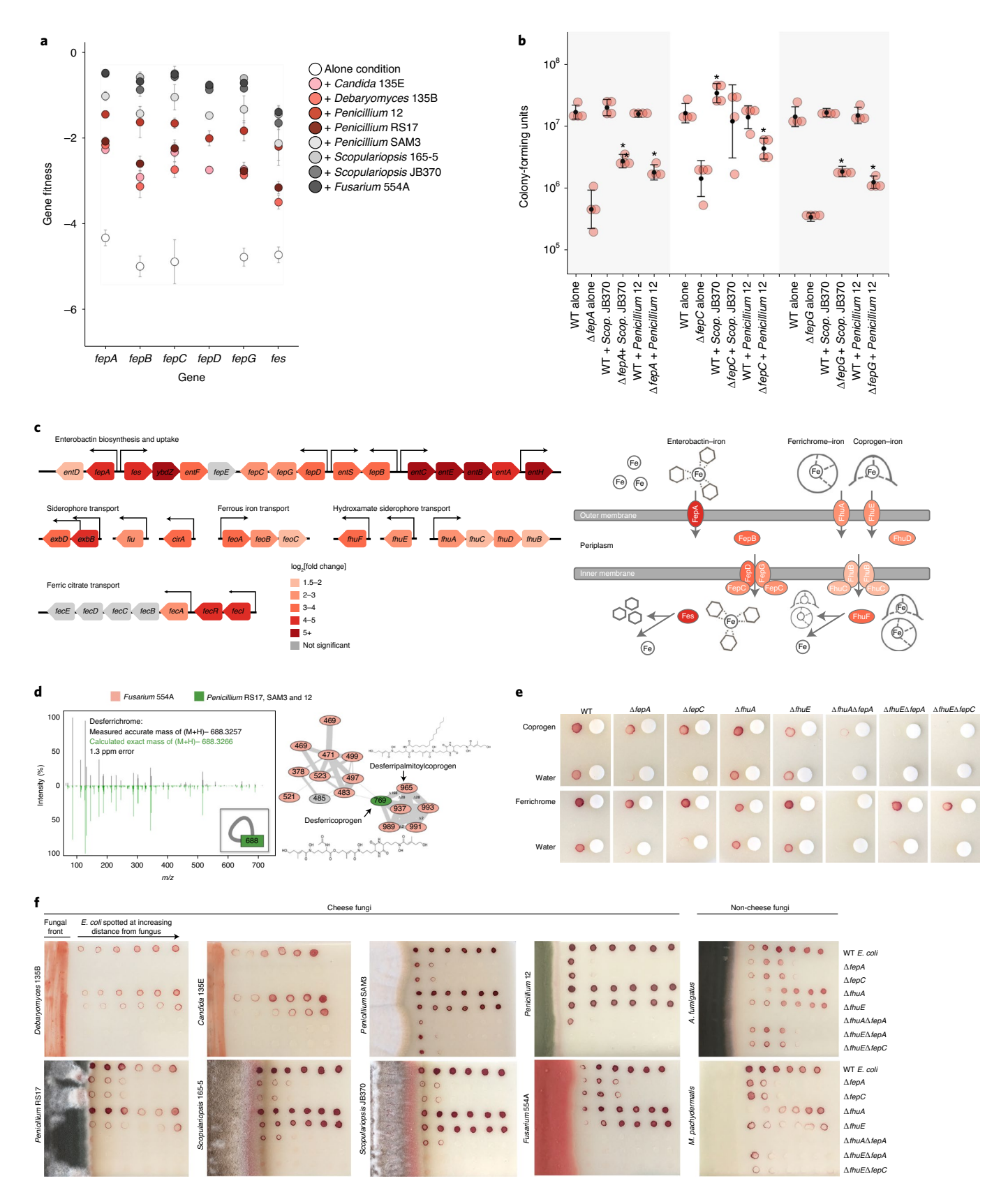
LC–MS comparison of WT and  $\Delta laeA$  Penicillium sp. str. 12 showed differential production of many metabolites, 94 of which showed a greater than tenfold change between the two (Supplementary Table 18). Of these, 93 were less abundant in the  $\Delta laeA$  mutant, which is consistent with the loss of secondary metabolite production in the  $\Delta laeA$  mutant (Fig. 6d). Cyclopenol, a biosynthetic intermediate for viridicatol<sup>43</sup>, was the only molecule reported to have antibiotic activity identified in the LC–MS data; it was produced by the WT Penicillium sp. str. 12 in more than tenfold higher quantity than  $\Delta laeA$ . However, further work is needed to determine whether this molecule is related to the antibacterial activity seen in BCP. In summary, these data highlight an important diminution of specialized metabolite production in the  $\Delta laeA$  strain.

Fig. 5 | Utilization of fungal siderophores by E. coli. a, RB-TnSeq fitness values for fep operon genes in alone or with fungi conditions showing an increase in fitness in the presence of fungal species. Fitness values are not shown for nonsignificant differences from alone condition. Error bars show the standard deviation of fitness values from the mean.  $\mathbf{b}$ , Colony-forming units of WT E. coli and  $\Delta fep$  mutants after 7 days of 1:1 competitive growth on CCA, pH7. Competitions between the two E. coli strains were performed with either no fungus present (alone) or with Penicillium sp. str. 12 or Scopulariopsis sp. str. JB370 (Scop. JB370). n = 4 biologically independent experiments, and error bars show the standard deviation from the mean (black circle). Asterisks indicate significantly different growth in the presence of a fungus relative to growth without the fungus (alone) based on a two-sided two-sample t-test P < 0.05. Exact P values associated with asterisks are as follows (from left to right): 0.001, 0.007, 0.034, 0.022, 0.0001 and 0.0006. c, E. coli iron-related genes upregulated in the presence of Penicillium sp. str. 12. Significance cut-off was made at abs(log<sub>2</sub>[fold change]) > 1.5 and adjusted P < 0.05. Differential expression analysis was performed using the default function DESeq87, which performs a Wald test with Benjamini-Hochberg75 correction for multiple comparison testing. Exact P values are available in Supplementary Table 14. The schematic on the right displays key proteins involved in siderophore uptake in E. coli. These proteins are coloured based on the upregulation of their corresponding genes. Fes and FhuF aid in removal of iron from siderophores inside the cell. d, Fungal siderophores identified by MS. The inset in the left box shows the node that represents the desferrichrome fragmentation pattern depicted, while the network on the right represents coprogen-related molecules. Coprogen B and ferrichrome were found by matching fragmentation patterns to library spectra. Both identifications were confirmed using retention time and fragmentation matching to a purchased standard. e, Visual assays of  $\Delta$ fep mutant growth with purified siderophores coprogen and ferrichrome. **f**, Visual assays of *E. coli* mutant growth at varying distances from pre-cultured cheese fungi, A. fumigatus (soil, human pathogen) and M. pachydermatis (skin commensal). For e and f, growth was performed on CCA. Tetrazolium chloride, a red indicator of cellular respiration, was added to the medium to visualize colony growth on the opaque CCA.

#### Discussion

Fungi have the potential to strongly affect bacterial neighbours in diverse systems, from soil to polymicrobial infections<sup>44–48</sup>. We combined the high-throughput genetic screen RB-TnSeq with BCP,

RNA-seq and metabolomics to identify a diversity of bacterial genes involved in, and the associated fungal contributors to, bacterial-fungal interactions in our system. This study provides new insight into the wide range of fungal impacts on bacteria that can occur



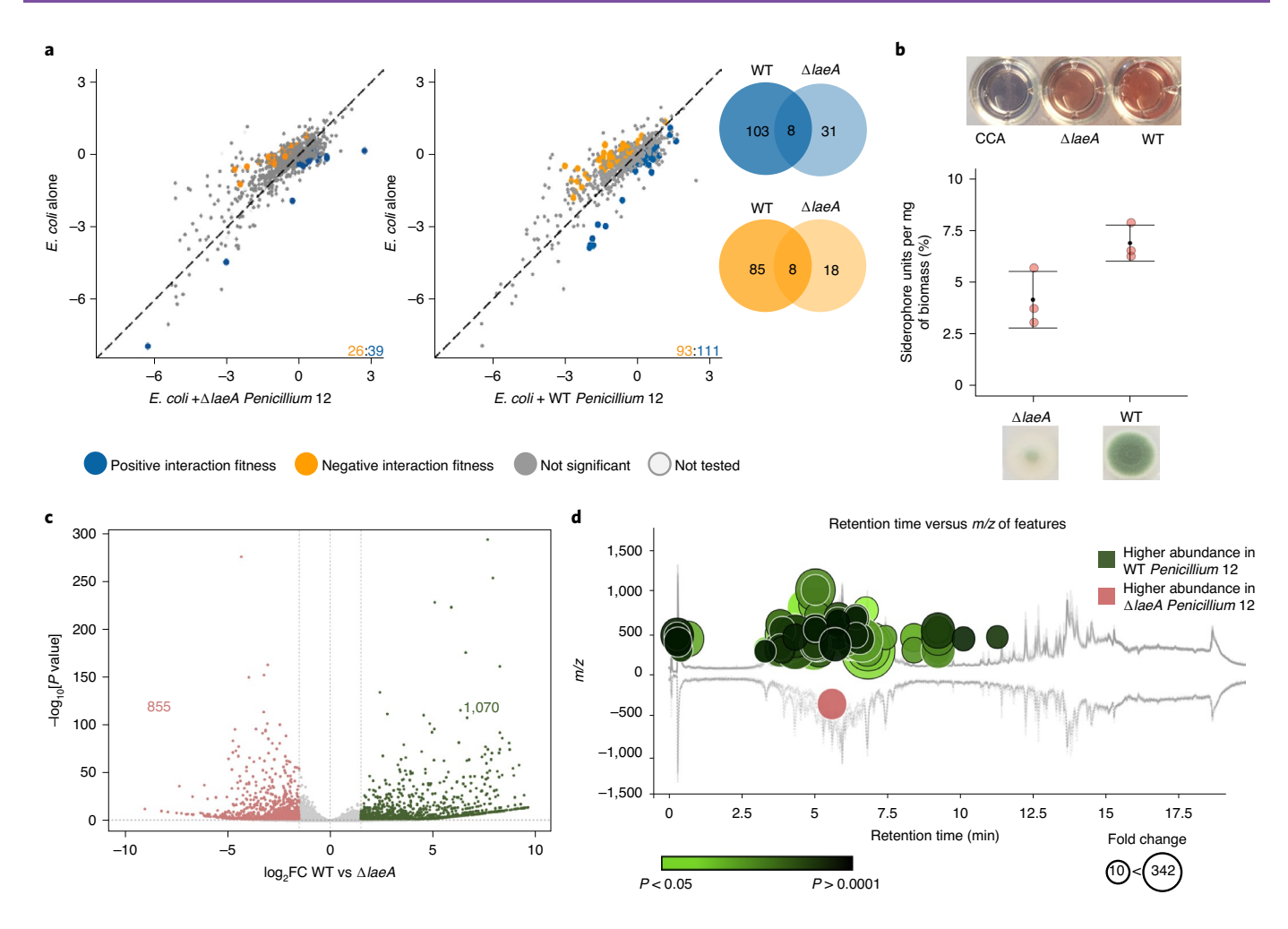


**Fig. 6 | Fungal metabolite production affects bacterial-fungal interactions. a**, *E. coli* genes with significant interaction fitness with  $\Delta laeA$  or WT *Penicillium* sp. str. 12. Each point represents a gene, with coloured points indicating genes with interaction fitness. The *x* and *y* values (plus fungal partner on the *x* axis; alone on *y* axis) indicate gene fitness values in each condition, and the numbers in the lower right-hand corner indicate how many genes have either positive (blue) or negative (orange) interaction fitness. The Venn diagrams display the overlap of these gene sets. **b**, Liquid CAS assay of supernatants from blank control CCA medium,  $\Delta laeA$  or WT *Penicillium* sp. str. 12 normalized to fungal biomass. n=3 biologically independent experiments, and error bars show the standard deviation from the mean. The asterisk indicates significantly different siderophore production (two-sided two-sample *t*-test, P=0.04). **c**, Differential expression of WT *Penicillium* sp. str. 12 relative to  $\Delta laeA$  after 3 days of growth on CCA. Labelled on the volcano plot are the number of genes with a  $\log_2$  fold change (FC) of >1.5 (green) or < -1.5 (red) and adjusted P<0.05. Differential expression analysis was performed using the default function DESeq<sup>37</sup>, which performs a Wald test with Benjamini–Hochberg<sup>75</sup> correction for multiple comparison testing. **d**, The metabolomics data analysis platform XCMS<sup>100</sup> was used to compare features detected by LC-MS analyses of  $\Delta laeA$  and WT *Penicillium* sp. str. 12 extracts (two-sided Welch's *t*-test for unequal variances). Features of higher abundance in WT relative to  $\Delta laeA$  are depicted as green nodes on the top of the mirror plot, and features of lower abundance in WT relative to  $\Delta laeA$  are depicted as red nodes on the bottom. The node radius is proportional to the fold change of the detected features, and the colour intensity is dependent on the *P* value. The graph displays only those features with a *P* value less than or equal to 0.05, a

even in a relatively simple system with pairwise combinations of bacteria and fungi. Our study focused on fungi from Ascomycota because this phylum is abundant in cheese rinds, and therefore represents a small sampling of the full genomic and functional diversity across fungi. It remains to be seen how these interactions might change with a more diverse set of partners, in conditions with varying ratios of bacteria and fungi, in varied environmental conditions or with increasing community complexity.<sup>16</sup>

Our study highlighted several important areas that contribute to bacterial-fungal interactions. First, multiple lines of evidence suggest that cheese-isolated *Penicillium* species exhibit antibiotic-like activity, although the mechanism underlying this activity is currently unknown. Although *Penicillium* species produce a wide

range of specialized metabolites, detection of known antibiotics such as penicillin in food products is limited<sup>30</sup>. Second, we found an increased need for biotin biosynthesis in the presence of fungi, which suggests that there is fungal competition for available biotin. Previous studies have pointed to roles of B vitamins in bacterial–fungal and even plant–bacterial interactions<sup>49,50</sup>. Third, the strongest and most widespread bacterial–fungal interaction that we observed suggests that fungal species can dramatically modulate access to iron through the provision of fungal siderophores such as ferrichrome and coprogen. It has long been known that bacteria grown in isolation are able to take up purified fungal siderophores, but the ecological relevance of this putative interaction has not been demonstrated<sup>36,51</sup>. Our results demonstrate that this exchange takes

place between bacteria and filamentous fungi growing in a biofilm and that this exchange can have impacts on the competitive fitness of bacteria. Our data suggest that cheese-associated yeast species may alleviate bacterial iron limitation through a different mechanism, as we did not detect siderophore production by these species.

Owing to the importance of iron in bacterial physiology and the prevalence of fungi in microbial ecosystems, we expect that iron-based bacterial-fungal interactions are important in other microbiomes. For example, growth of non-siderophore-producing mutants of soil-dwelling Streptomyces coelicolor was restored by the presence of siderophores from airborne contaminant Penicillium<sup>52</sup>. Moreover, many filamentous fungi outside the genera studied here can produce siderophores<sup>53</sup>. In addition to filamentous fungi, we showed that the basidiomycete skin yeast M. pachydermatis alleviated bacterial iron limitation. Human skin microbiome yeasts Malassezia restricta and Malassezia globosa have previously been found to possess genes for siderophore biosynthesis<sup>54,55</sup>. Fungal growth may also be affected by inter-kingdom siderophore exchange, as some fungal species have evolved mechanisms of utilizing bacterial siderophores while others are inhibited by bacterial siderophores<sup>56-58</sup>.

FhuE and FhuA receptors are widespread in Proteobacteria, further suggesting that inter-kingdom siderophore exchange could play an important role in diverse systems. Hydroxamate siderophore uptake systems have also been identified in Gram-positive bacterial pathogens<sup>59,60</sup>. Additionally, hydroxamate siderophore uptake systems affect bacterial fitness, as shown in a murine infection model<sup>61</sup>. *Bacteroides fragilis*, a human gut symbiont, is able to use ferrichrome to grow in iron-limiting conditions, and *fhu* genes are expressed by *E. coli* in colonic mucus<sup>62,63</sup>. Fermented foods are known to contain fungal siderophores, which could be a source of fungal siderophores in the gut in addition to potential siderophore production by gut-resident species<sup>64,65</sup>.

We anticipated that by looking for fungal impacts on *E. coli*, we could leverage the genetic information available for this species. However, even in this well-characterized organism, 38% of genes identified as having interaction fitness are annotated as hypothetical, uncharacterized or putative. For *P. psychrophila*, 27% of genes with interaction fitness are hypothetical proteins. Similarly, the chemical identity and ecological relevance of most of the specialized metabolites we identified in our *Penicillium* species are unknown. This highlights that many genes and molecules involved in interspecies interactions are yet to be characterized, and that studying microbes in the context of their interactions with other species, and not just in monoculture, provides an avenue for uncovering new areas of biology.

# Methods

**Source information for strains and libraries.** Source information for strains and libraries used in this study is provided in Supplementary Table 19.

Sequencing of the fungal ribosomal RNA gene. Genomic DNA (gDNA) was extracted using phenol-chloroform (pH 8) from cultures of the eight cheese fungal species used in this study. For each extraction,  $125\,\mu l$  of  $425-600-\mu m$ acid-washed beads and 125 ul of 150-212-um acid-washed beads were poured into a screw-capped 2-ml tube. A total of 500 µl of 2× buffer B (200 mM NaCl, 20 mM EDTA) and 210 µl of SDS 20% were added to the tube containing fungal material and 500 µl of phenol-chloroform (pH 8). Cells were lysed by vortexing the tubes for 2 min at maximum speed. Aqueous and organic phases were separated by centrifugation at 4°C, 8,000 r.p.m. for 3 min, and 450 µl of the aqueous phase (upper phase) was recovered in a 1.5-ml Eppendorf tube. Sodium acetate  $(3\,M,\,45\,\mu l)$  and ice-cold isopropanol  $(450\,\mu l)$  were added before incubating the tubes at -80 °C for 10 min. The tubes were then centrifuged for 5 min at 4 °C at  $13,000\,r.p.m.$  The pellet was then washed in  $750\,\mu l$  of 70% ice-cold ethanol and resuspended in 50 µl of DNase/RNase-free water. Following DNA extraction, LROR (ACCCGCTGAACTTAAGC) and LR6 (CGCCAGTTCTGCTTACC)6 primers were used to amplify the large subunit of the ribosomal RNA, and for Penicillium species, Bt2a (GGTAACCAAATCGGTGCTTTC) and Bt2b  $(ACCCTCAGTGTAGTGACCCTTGGC)^{\it co}\ primers\ were\ used\ to\ amplify\ the$ 

β-tubulin gene. PCR was performed in a final volume of 50 μl (25 μl of Q5 polymerase master mix (New England Biolabs), 2.5 µl of the forward primer at 10 μM, 2.5 μl of the reverse primer at 10 μM, 100 ng of gDNA, and water) using the following PCR programmes: (1) for LSU: 98 °C for 30 s, then 35 cycles of 98 °C for 10 s, 52 °C for 30 s, followed by 72 °C for 1.5 min, and finally 72 °C for 5 min; (2) for β-tubulin: 98 °C for 30 s, then 35 cycles of 98 °C for 10 s; 57 °C for 30 s, followed by 72 °C for 1 min, and finally, 72 °C for 5 min. PCR products were purified using a QIAquick PCR purification kit (Qiagen) and sequenced using the forward and reverse primers by Eton Bioscience. Consensus sequences from forward and reverse sequencing reactions of the LROR/LR6 PCR product were aligned using Geneious v.R9 9.1.8 (http://www.geneious.com). The MrBayes68 plugin for Geneious was used to build the phylogenetic tree with the following parameters: Substitution model- JC69; Rate variation- gamma; Outgroup- Fusarium sp. str. 554A; Gamma categories-4; Chain Length- 1100000; Subsampling freq- 200; Heated chains-4; Burn-in length- 100000; Heated chain temp- 0.2; Random seed-1160; Unconstrained branch lengths- 1, 0.1, 1, 1. FigTree v.1.4.4 was used for visualization (https://github.com/rambaut/figtree/releases).

Bacterial–fungal growth assays. To approximate a 1:1 ratio of bacteria and fungi based on cell size, we inoculated 60,000 bacterial cells alone or with 6,000 fungal spores per well on 10% CCA medium²s adjusted to pH7 in a 96-well plate. Each bacterial or bacterial–fungal assay was done in triplicate. After 7 days of growth at room temperature, the entire well was collected and homogenized in 1×PBS–Tween 0.05% before dilution and plating on LB medium with 20 μg ml $^{-1}$  cycloheximide (for bacterial counts) or plate count agar supplemented with 0.1% milk and 1% salt (PCAMS) with 50 μg ml $^{-1}$  chloramphenicol (for fungal spore counts). Counts were done at inoculation and after collection. Final growth counts were then compared between the co-culture condition relative to growth alone to identify interaction effects. Significant growth effects were determined based on Dunnett's test. P<0.05. Plots were made using the R package ggplot (v.2 3.2.1) $^{70}$ .

Microbial culturing for LC–MS/MS extraction. All fungal cultures were grown on PCAMS. Plates were kept at room temperature and spores were collected at 7 days of growth (or after sporulation was observed) for subsequent experiments. Spores collected from fungi were normalized to an optical density at  $600\,\mathrm{nm}$  (OD  $_{600}$ ) of 0.1 in PBS for a working stock.

Extraction of cultures. Three biological replicates of each condition were plated (distinct samples) and extracted from solid agar. For extraction from solid agar plates, 5µl of fungal working stock was spotted onto 10% CCA medium adjusted to pH7. Following 7 days of growth, agar was removed from the Petri dish and placed into 50-ml Falcon tubes. Acetonitrile (10 ml) was added to each tube and all were sonicated for 30 min. All Falcon tubes were centrifuged, and liquid was removed from the solid agar pieces and transferred to 15-ml Falcon tubes. The 15-ml Falcon tubes containing liquid were then centrifuged and liquid was again removed from any residual solid debris and transferred to glass scintillation vials. These liquid extractions were then dried in vacuo. Dried extracts were weighed and diluted with methanol to obtain 1 mg ml<sup>-1</sup> solutions, which were stored at -20 °C until analysis via LC-MS/MS.

LC–MS/MS data collection. High-resolution LC–MS and LC–MS/MS data were collected on a Bruker impact II qTOF in positive mode with the detection window set from 50 to 1,500 Da on a 2.1  $\times$  150-mm C18 Cortecs UPLC column with a flow rate of 0.5 ml min $^{-1}$  for a gradient of 10–100% acetonitrile with 0.1% formic acid over 16 min. For each sample, 10  $\mu$ l of a 1 mg ml $^{-1}$  solution was injected. The electrospray ionization conditions were set with the capillary voltage at 4.5 kV. For MS $^2$ , dynamic exclusion was used, and the top nine precursor ions from each MS $^1$  scan were subjected to collision energies scaled according to the mass and charge state for a total of nine data-dependent MS $^2$  events per MS $^1$ . MS $^2$  data for pooled biological replicates have been deposited under MassIVE accession number MSV000085070. MS $^1$  and MS $^2$  data for  $\Delta laeA$  and WT Penicillum sp. str. 12 have been deposited under MassIVE accession number MSV000085054 and were collected under identical conditions on a Bruker compact qTOF.

Molecular networking. For all extractions, all precursor m/z values that were found in solvent and agar controls (based on both retention time and mass tolerance) were removed before input into Global Natural Products Social molecular networking (GNPS) using the BLANKA algorithm<sup>71</sup>. A molecular network (https://gnps.ucsd.edu/ProteoSAFe/status.jsp?task=464b331ef9d54de995 7d23b4f9b9db14) was created using the online workflow in GNPS. The data were filtered by removing all MS/MS peaks within ±17 Da of the precursor m/z. MS/MS spectra were window filtered by choosing only the top six peaks in the ±50-Da window throughout the spectrum. The data were then clustered with MS-Cluster with a parent mass tolerance of 0.02 Da and a MS/MS fragment ion tolerance of 0.02 Da to create consensus spectra. Furthermore, consensus spectra that contained fewer than two spectra were discarded. A network was then created whereby edges were filtered to have a cosine score above 0.7 and more than six matched peaks. Further edges between two nodes were kept in the network only if each of the nodes appeared in each other's respective top ten most similar nodes. The spectra

in the network were then searched against the spectral libraries of the GNPS. The library spectra were filtered in the same manner as the input data. All matches kept between network spectra and library spectra were required to have a score above 0.7 and at least six matched peaks. Solvent and agar control files were also loaded into the networks to perform removal based on fragmentation patterns. All nodes with precursor masses less than 200 Da were also removed. The extensive background and low m/z Da value removal was done to more accurately reflect the metabolomic profiles of fungal genera in an attempt to represent only true metabolites. The Dereplicator algorithm  $^{72,73}$  was used to annotate MS/MS spectra. The molecular networks were visualized using Cytoscape software  $^{74}$ .

RB-TnSeq assays. All RB-TnSeq assays were performed on 10% CCA medium adjusted to pH7. Before inoculation, one aliquot of each library was thawed and inoculated into 25 ml of liquid LB with kanamycin (50 μg ml<sup>-1</sup>). This is the same medium used for creating the initial library and is expected to be nonselective. Once the culture reached mid-log phase (OD = 0.6-0.8), 5 ml of that pre-culture was pelleted and stored at -80 °C for the T0 reference in the fitness analysis. The remaining cells were used to inoculate the fitness assay conditions. For each RB-TnSeq fitness assay, we aimed to inoculate 7,000,000 cells of the bacterial library (on average 50 cells per insertion mutant). For fitness assays including a fungal partner, 700,000 fungal cells were inoculated based on spore counts. We inoculated ten times more bacterial cells than fungal spores to approximate a 1:1 volume ratio of bacteria:fungi, as fungal cells are approximately ten times larger than bacterial cells. Pre-cultured cells were washed in 1×PBS-Tween 0.05%, mixed with appropriate volumes of quantified fungal spore stocks, and then inoculated by spreading evenly on a 100-mm Petri dish containing 10% CCA medium, pH7. For each condition, assays were performed in triplicate (three distinct samples). After 7 days, each plate was flooded with 1.5 ml of 1×PBS-Tween 0.05% and cells were scraped off, taking care not to disturb the CCA. The liquid was then transferred into a 1.5-ml microcentrifuge tube and cells were pelleted by centrifugation. After removing the supernatant, the cells were washed in 1 ml of RNAprotect solution (Qiagen), pelleted and stored at -80°C until gDNA extraction. gDNA was extracted with phenol-chloroform (pH 8) using the same protocol used for fungal gDNA extraction described above. Samples were stored at -80°C until further analysis.

After gDNA extraction, extracts containing Penicillium sp. str. 12 DNA were purified using a OneStep PCR Inhibitor Removal kit (Zymo Research). Then, the 98 °C BarSeq PCR protocol as previously described in Wetmore et al. 18 was used to amplify only the barcoded region of the transposons. PCR was performed in a final volume of 50 µl with the following content: 25 µl of Q5 polymerase master mix (New England Biolabs), 10 µl of GC enhancer buffer (New England Biolabs), 2.5 µl of the common reverse primer (BarSeq\_P1 - Wetmore et al. 18) at 10 µM, 2.5 µl of a forward primer from the 96 forward primers (BarSeq P2 ITXXX) at  $10\,\mu\text{M}$  and either 200 ng of gDNA for growth-alone conditions or  $2\,\mu\text{g}$  of gDNA for fungal interaction conditions. For E. coli analysis, we performed 84 PCR assays (T0 sample and 28 collected samples in triplicate) involving 28 different multiplexing indices. For P. psychrophila str. JB418 analysis, we performed 84 PCR assays (T0 sample and 28 collected samples in triplicate) involving 28 different multiplexing indices. We used the following PCR programme: (1) 98 °C for 4 min; (2) 30 cycles of 98 °C for 30 s, 55 °C for 30 s and 72 °C for 30 s; and (3) 72 °C for  $5\,\mathrm{min}.$  After the PCR, for both E. coli and P. psychrophila,  $10\,\mu\mathrm{l}$  of each of the PCR products was pooled together to create the BarSeq sequencing library, and 200 µl of the pooled library was purified using a MinElute purification kit (Qiagen). The final elution of the BarSeq library was performed in  $30\,\mu l$  of DNase- and RNase-free water. The BarSeq libraries were then quantified using a Qubit dsDNA HS assay kit (Invitrogen) and sequenced on a HiSeq4000 (75 bp, single-end reads) by the IGM Genomics Center at the University of California, San Diego. The sequencing depth for each condition varied between 6.1 and 11.7 million reads for E. coli and 5.8 and 13.3 million reads for P. psychrophila.

RB-TnSeq data processing. Custom R scripts were used to determine the average fitness scores for each gene across three RB-TnSeq assay replicates. These scripts  $are\ available\ at\ https://github.com/DuttonLab/RB-TnSeq-Microbial-interactions.$ The Readme document provides an in-depth explanation of all the data processing steps performed in these scripts. Insertion mutants that did not have a sufficient T0 count (3) in each condition or that were not centrally inserted (10-90% of gene) were removed from the analysis. Counts as determined using the scripts described by Wetmore et al.18 were then normalized using a set of five reference genes (glgP, acnA, modE, leuA and idnK in E. coli (average of 52 strains each) and the respective closest protein BLAST matches Ga0212129\_11488, Ga0212129\_114557, Ga0212129\_111416, Ga0212129\_112128 and Ga0212129\_112491 (average of 74 strains each) in P. psychrophila) to be able to compare across conditions and to account for differences in sequencing depth. These genes have an absolute fitness effect of <0.6 in all conditions for all replicates in any condition based on a former fitness determination developed by Wetmore et al. 18. Strain fitness ( $f_s$ ) was then calculated per insertion mutant as the  $\log_2$  of the ratio of the normalized counts in the condition and the normalized counts in the T0 sample (equation (1)).

$$f_{\rm s} = \log_2(\frac{Cc}{Ct0}) \tag{1}$$

with Cc representing normalized counts in condition C and Ct0 representing normalized counts in T0.

Gene fitness and variance were next calculated by averaging insertion mutants within a gene. These values were then normalized based on the position of the gene along the chromosome using a smoothed median on a window of 251 genes as described in Wetmore et al.  $^{18}$ . These steps were all done on individual replicates. For all conditions, replicates were highly correlated, with an averaged Pearson correlation coefficient of 0.85 for  $E.\ coli$  and 0.84 for  $P.\ psychrophila.$  Next, the average gene fitness  $(f_g)$  (equation (2)) and associated standard deviation  $(\sigma_g)$  (equation (3)) were calculated using the inverse of variance weighted average of the fitness values across the three different replicates.

$$f_{g} = \frac{\sum_{i=1}^{n} w_{i} \times f_{g_{i}}}{\sum_{i=1}^{n} w_{i}}$$
 (2)

$$\sigma_{\mathbf{g}} = \sqrt{\left(\frac{n}{n-1}\right) \times \left(\frac{\sum_{i=1}^{n} w_{i} \times \left(f_{\mathbf{g}} - \underline{f_{\mathbf{w}\underline{\mathbf{g}}}}\right)^{2}}{\sum_{i=1}^{n} w_{i}}\right)}$$
(3)

With  $w_i$  representing the inverse of the gene fitness variance for each replicate, n the number of replicates and  $f_{wg}$  the weighted gene fitness average across the n replicates.

Final fitness values were then compared between fungal interaction conditions and bacteria alone conditions using two-sided *t*-tests (when the equality of variance was verified by Fisher test) and correction for multiple comparison (Benjamini–Hochberg method<sup>78</sup>). Comparisons associated with an adjusted *P* value lower than 5% were considered a significant interaction fitness (alphaF parameter=0.002 and alphaT parameter=0.05 in Script3\_2conditions\_FitnessComparison.Rmd code). The overall pipeline is described in Extended Data Fig. 1, and Supplementary Method 1 provides an example for a complete run. Networks of fitness values were visualized in Cytoscape (v.3.5.1)<sup>74</sup>, and principal component analysis plots were made using the R packages ggplot2 (v.3.2.1)<sup>70</sup> and ggfortify (v.0.4.7)<sup>70</sup>. COG category mapping of *E. coli* and *P. psychrophila* protein sequences was done using eggNOG-mapper (v.2)<sup>77</sup>.

Functional enrichment analysis of bacterial gene sets. Cluster Profiler \*\* was used for GO functional enrichment analysis of bacterial gene sets with a false discovery rate *P* value adjustment cut-off of 0.1. For *E. coli*, the *E. coli* K12 database (org.EcK12.eg.db) \*\* was used. For *P. psychrophila*, a custom annotation database was created using eggNOG-mapper v.2 (ref. \*\*\*) GO assignments using AnnotationForge\*\* in R.

Bacterial cytological profiling. Approximately 7,000,000 WT E. coli K12 strain BW25113 or Keio collection mdtK mutant cells81 were inoculated alone or co-inoculated with 700,000 Penicillium sp. str. 12, Penicillium sp. str. 12 ΔlaeA or Penicillium sp. str. SAM3 spores on 10% CCA pH7. After 7 days of growth, 1 ml of T-Base buffer was added to the surface of the biofilms, and biofilms were scraped into the buffer. For co-culture conditions, the sample was filtered through a 0.5-um filter to specifically remove fungal material. A total of 2  $\mu$ l of concentrated dye mix (1  $\mu$ l of 1 mg ml $^{-1}$  FM4-64, 1  $\mu$ l of 2 mg ml $^{-1}$ 4,6-diamidino-2-phenylindole (DAPI) in 48 µl of T-Base) was added to 20 µl of filtrate. The dye filtrate mix was spotted onto agarose-LB pads (1% agarose, 20% LB liquid medium, 80% ddH<sub>2</sub>O) and imaged by fluorescence and phase contrast microscopy using an Applied Precision Deltavision Spectris imaging system with an Olympus UPLFLN100XO2PH objective. Control compound references on CCA medium were obtained by spotting and drying 30 µl of 5-, 10-, 25- and 100-times minimum inhibitory concentration dilutions of antibiotics onto quadrants on CCA medium pH7 plates and then spread-plating 200 µl of log-phase (OD of 0.1) E. coli cultures. After 2 days of growth, cells near the edge of the zone of inhibition on appropriate dilution spots were resuspended in 10 µl of prediluted dye mix (1 µl 1 mg ml-1 FM4-64, 1 µl 2 mg ml-1 DAPI in 998 µl of T-Base) and spotted onto agarose-LB pads and imaged as described above. Resulting images were deconvoluted using Deltavision SoftWorx software (Applied Precision), analysed using Fiji82 and assembled in Adobe Photoshop (Adobe). Brightness was altered linearly in Fiji to aid visualization. For quantification of cell roundness, we defined the cell major axis as the longest possible line along the cell, and the cell minor axis was measured as the longest possible line orthogonal to the cell major axis. Cell measurements were obtained via the measure tool in Fiji82, and single-cell major and minor axes measurements were collated. The pixel to micron ratio was set as 15.6 as per the microscope specifications. The major/minor axis ratio was calculated for all cells in the field. The number of fields was chosen to ensure measurement of at least 50 cells for each experimental condition. Individual ratio values for each cell were plotted via the R package ggplot2 (v.3.2.1)70, and differences in major/minor ratios in the presence of a fungus relative to growth alone or with WT *Penicillium* sp. str. 12 relative to  $\Delta laeA$  Penicillium sp. str. 12 were determined based on an unpaired two-sample Wilcoxon test P < 0.05.

CCA medium biotin quantification. Biotin quantification of CCA medium was performed on three replicate samples by Creative Proteomics as follows:  $100\,mg$  of each sample was homogenized in water  $(10\,\mu l\,mg^{-1})$  for 1 min three times with the aid of 5-mm metal balls on a MM400 mill mixer. Methanol  $(10\,\mu l\,mg^{-1})$  was then added. Water-soluble vitamins were extracted by vortex mixing for 2 min and sonication in a water batch for 5 min. After centrifugation, the clear supernatants were cleaned up by solid-phase extraction on a Strata-X (60 mg ml^{-1}) cartridge. The eluted fractions containing water-soluble vitamins were collected, pooled and then dried under a gentle nitrogen gas flow in a nitrogen evaporator. The residues were dissolved in 200  $\mu$  of 10% methanol. Aliquots (20  $\mu$ l) were injected to run on a UPLC–MRM/MS with the use of a C18 UPLC column and with (+) ion detection and (–) ion detection. Calibration curves were prepared by injection of serially diluted mixed standard solutions of water-soluble vitamins. Concentrations of detected vitamins were calculated by interpolating the linear calibration curves.

 $\Delta fep$  mutant competitive growth assays. Approximately 60,000 bacterial cells (a 1:1 ratio of WT cells and  $\Delta fepA, \Delta fepC$  or  $\Delta fepG$  Keio collection  $^{81}$  mutant cells) were inoculated either alone (no fungus) or co-inoculated with approximately 6,000 Penicillium sp. str. 12 or Scopulariopsis sp. str. JB370 spores on 10% CCA pH7 in a 96-well plate in four replicates each (four distinct samples). After 7 days of growth, the entire well was collected and homogenized in 1×PBS–Tween 0.05% before dilution and plating on LB with 20  $\mu g\,ml^{-1}$  cycloheximide (total bacterial counts) or with 20  $\mu g\,ml^{-1}$  cycloheximide and 50  $\mu g\,ml^{-1}$  kanamycin (bacterial mutant counts). Final growth counts were then compared in fungal co-culture conditions relative to bacterial growth alone to identify interaction effects. Significant growth effects were determined by significantly different growth in the presence of a fungus relative to growth alone based on a two-sided two-sample t-test P < 0.05. Plots made using the R package ggplot2 (v.3.2.1)  $^{70}$ .

**Siderophore detection with CAS assays.** The following methods were adapted from those described by Schwyn and Neilands<sup>83</sup> and Payne<sup>84</sup>. All glassware, caps and stir bars were cleaned with 6 M HCl and rinsed with deionized water. Plastic spatulas and doubly deionized water were used for solution preparation. A 2 mM CAS stock solution was prepared and stored in the dark at room temperature, and a 1 mM FeCl<sub>3</sub> stock solution was prepared. Piperazine buffer was prepared by dissolving 4.3095 g of anhydrous piperazine in 30 ml of water and adding 5 M HCl until the pH reached 5.635. To prepare the CAS reagent, 1.1202 ml of 0.05 M hexadecyltrimethylammonium bromide (HDTMA) was added to 50 ml of water. Then, 1.5 ml of 1 mM FeCl<sub>3</sub> stock solution was mixed with 7.5 ml of 2 mM CAS solution and added to the HDTMA solution. Last, the piperazine buffer was added to the solution and stirred. The resulting CAS assay solution was stored in the dark at room temperature. A 0.2 M shuttle solution was prepared with 5-sulfosalicylic acid dihydrate in water. The shuttle solution was stored in the dark at room temperature.

For detection of siderophore presence, fungal species were inoculated in triplicate into liquid 2% CCA pH7, and cultures were grown at room temperature for 12 days. For filamentous fungi, cultures were left standing without shaking. After 12 days, supernatants were filtered through a 0.22-µm filter. Before use, the CAS assay solution was vortexed until all precipitates were resuspended. CAS assay incubations were performed in the dark at room temperature. For each fungal supernatant or CCA filtrate,  $100\,\mu l$  of CAS assay solution was added to  $100\,\mu l$  of supernatant. The resulting solution was mixed by pipetting and incubated for 15 min. After incubation,  $2\,\mu l$  of shuttle solution was added to the solution and mixed by pipetting. The solution was incubated for an additional 30 min. Sample absorbance of 630-nm light was measured in a 96-well plate using an Epoch 2 plate reader (BioTek).

For CAS assay comparisons of relative siderophore production in WT and  $\Delta laeA$  Penicillium sp. str. 12, 200,000 spores of WT or  $\Delta laeA$  were inoculated in triplicate in 3 ml of liquid 2% CCA pH7. After 7 days of growth at room temperature without shaking, the biomass of the fungal mat was removed from the top of the culture and the entire supernatant was filtered through a 0.22-µm filter. Total filtrate was measured. Fungal mats were dried in a 60 °C drying oven for 2 days before being weighed. Filtrates were concentrated 3× in a SpeedVac Vacuum Concentrator and 100 µl of three replicates each of WT,  $\Delta laeA$  and 2% liquid CCA were added to 100 µl of CAS solution, and CAS assays were performed as described above. Following CAS measurements, the percentage siderophore units were normalized to the entire volume of 1× filtrate and expressed as per mg of dried fungal biomass.

RNA-seq and differential expression analysis of *E. coli* with *Penicillium* sp. str. 12. Approximately 7,000,000 *E. coli* cells were inoculated in triplicate (three distinct samples) either alone or with approximately 700,000 *Penicillium* sp. str. 12 spores on 10% CCA pH7 in standard petri dishes. After 3 days, the biofilms were collected for RNA extraction and washed with 1 ml of RNAprotect. RNA was extracted by a phenol–chloroform extraction (pH8) using the same extraction protocol as for gDNA. Extractions were then purified using a OneStep PCR Inhibitor Removal kit (Zymo Research).

Sequencing libraries were prepared as follows: RNA samples were treated with DNase using the 'Rigorous DNase treatment' for the Turbo DNA-free kit (Ambion, Life Technologies), and the RNA concentration was measured by nucleic

acid quantification in an Epoch microplate spectrophotometer (BioTek). Transfer RNAs and 5S RNA were then removed using a MEGAclear kit Purification for Large Scale Transcription Reactions (Ambion, Life Technologies) following the manufacturer's instructions. Absence of tRNA and 5S RNA was verified by running 100 ng of RNA on a 1.5% agarose gel, and the RNA concentration was quantified by nucleic acid quantification in an Epoch microplate spectrophotometer. Also, the presence of gDNA was assessed by PCR using universal bacterial 16S PCR primers (forward primer: AGAGTTTGATCCTGGCTCAG; reverse primer: GGTTACCTTGTTACGACTT). The PCR was performed in a final volume of 20  $\mu$  (10  $\mu$ ) of Q5 polymerase master mix (New England Biolabs), 0.5  $\mu$ l of forward primer 10  $\mu$ M, 0.5  $\mu$ l of reverse primer 10  $\mu$ M and 5  $\mu$ l of non-diluted RNA). PCR products were run on a 1.7% agarose gel and if gDNA was amplified, another DNase treatment was performed as well as a new verification of absence of gDNA.

Ribosomal RNA depletion was performed using a RiboMinus Transcriptome Isolation kit (yeast and bacteria) for the E. coli alone samples and using both a RiboMinus Transcriptome Isolation kit (yeast and bacteria) and a RiboMinus Eukaryote kit v.2 for the mixed E. coli-Penicillium sp. str. 12 samples (ThermoFisher Scientific). For the E. coli alone samples, each sample was divided into two for treatment and then repooled for RNA recovery with ethanol precipitation. For the E. coli-Penicillium sp. str. 12 samples, an equal volume of the eukaryotic probe and RiboMinus Bacterial Probe Mix were used to deplete both bacterial and fungal ribosomal RNA, and RNA was recovered by ethanol precipitation. Concentrations after ribosomal RNA depletion were measured using Qubit RNA HS Assay kits (Invitrogen). The RNA-seq library was produced using a NEBNext Ultra RNA Library Prep kit for Illumina for purified mRNA or ribosome-depleted RNA. We prepared a library with a fragment size of 300 nucleotides and used the 10 µM NEBNext Multiplex Oligos for Illumina (Set 1, NEB E7335, lot 0091412) and the NEBNext multiplex Oligos for Illumina (Set 2, NEB E7500, lot 0071412). We performed PCR product purification with 0.8× Agencourt AMPure XP Beads. Library samples were quantified using Qubit DNA HS Assay kits before the quality and fragment size were validated by TapeStation (HiSensD1000 ScreenTape). Library samples were pooled at a concentration of 15 nM each and were sequenced on a HiSeq4000 (50 bp, single-end). TapeStation assays and sequencing were performed by the IGM Genomics Center at the University of California, San Diego.

Following sequencing, reads were mapped to the concatenated genome of *E. coli* K12 BW25113 (ref. <sup>85</sup>) and *Penicillium* sp. str. 12 using Geneious v.R9 9.1.8 (http://www.geneious.com). Only the reads that uniquely mapped to a single location on the *E. coli* genome section were kept. *E. coli* expression analysis was performed using the following R packages: Rsamtools (R package v.2.0.3), GenomeInfoDb (R package v.1.20.0), GenomicFeatures<sup>86</sup> (R package v.1.36.4), GenomicAlignments<sup>86</sup> (R package v.1.20.1), GenomicRanges<sup>86</sup> (R package v.1.36.1) and DESeq2 (ref. <sup>87</sup>) (R package v.1.20.1). We followed the workflow described by Love et al. 2014 (ref. <sup>87</sup>) and performed the differential expression analysis using the package DESeq2. Differentially expressed genes between conditions were selected using an adjusted *P* value lower than 5% (Benjamini–Hochberg correction for multiple testing<sup>75</sup>) and an absolute log, fold change equal to or greater than 1.5.

Construction of *E. coli* mutants and visual interaction assays. *Visual assays for purified hydroxamate siderophore stimulation*. Antibiotic assay discs (Whatman) were placed on CCA medium pH 7 with 0.005% tetrazolium chloride (an indicator of cellular respiration) and 20 µl of water, or  $10\,\mu\text{M}$  coprogen or ferrichrome (EMC Microcollections) solutions (in water) were slowly pipetted onto the disc and allowed to absorb. Aliquots (2.5 µl) of 37 °C overnight LB cultures of *E. coli* K12 BW25113 WT,  $\Delta fepA$ ,  $\Delta fepC$ ,  $\Delta fhuE$ ,  $\Delta fhuA$ ,  $\Delta fepA\Delta fhuE$ ,  $\Delta fepC\Delta fhuE$  or  $\Delta fepA\Delta fhuA$  mutants were spotted next to the discs. Double mutants were constructed as described below. Plates were left at room temperature until development of red colour resulting from tetrazolium chloride, an indicator of respiration.

Visual assays for fungal stimulation of bacterial mutants. Fungal spores were inoculated on CCA pH7 with 0.005% tetrazolium chloride. After fungal pre-culturing at room temperature (cheese fungal isolates) or 30 °C (A. fumigatus and M. pachydermatis), 2.5 µl of E. coli overnight cultures grown in LB medium at 37 °C were spotted at increasing distances from the fungal front. Plates were left at room temperature until red colour developed. The A. fumigatus isolate AF293 was received from N. Keller, University of Wisconsin–Madison. M. pachydermatis was originally isolated from the ear of a dog in Sweden (ATCC14522 from ATCC).

Creation of  $\Delta fepA\Delta fhuE$  and  $\Delta fepC\Delta fhuE$ . Chemically competent cells for  $\Delta fepA$  or  $\Delta fepC$  mutants were created. An overnight culture of  $\Delta fepA$  or  $\Delta fepC$  mutants was diluted 1:100 and grown at 37 °C until OD of 0.4–0.6. The culture was placed on ice for 20 min and then centrifuged at 4 °C for 10 min at 6,000 r.p.m. to collect the cells. The supernatant was removed, and cells were resuspended in half the previous volume of pre-cooled 0.1 M CaCl<sub>2</sub>. After incubating on ice for 30 min, centrifugation was repeated, and supernatant was removed before resuspension in one-quarter of the original volume of pre-cooled 0.1 M CaCl<sub>2</sub>/15% glycerol. Cells were aliquoted and stored at -80 °C until transformation. These cells were transformed with the pKD46 plasmid<sup>88</sup>, recovered at 30 °C, and plated

on LB plates with 100 µg ml<sup>-1</sup> ampicillin and grown at 30 °C. Overnight cultures were started from individual colonies for the creation of electrocompetent cells. Overnight cultures of  $\Delta fepC$ -pkD46 or  $\Delta fepA$ -pkD46 were diluted 1:100 in fresh LB with 100 µg ml<sup>-1</sup> ampicillin and grown at 30 °C until an OD of 0.1. A total of 20 µl of fresh 1 M L-arabinose was added, and growth was continued at 30 °C until OD 0.4-0.6. Cells were then chilled on ice for 15 min and then centrifuged for 10 min at 4,000 r.c.f. at 4 °C. Cells were resuspended in 1 ml of ice water and centrifuged for 10 min at 4,000 r.c.f. at 4 °C. Cells were resuspended in 0.5 ml of ice water and centrifuged for 10 min at 4,000 r.c.f. at 4 °C. Cells were resuspended in  $50\,\mu l$  of ice water and kept on ice until transformation. The chloramphenicol resistance cassette was amplified from the pKD3 plasmid88 using the following custom primers: FhuEcatF (CAGATGGCTGCCTTTTTTACAGGTGTTATTCA-GAATTGATACGTGCCGGTAATGGCGCGCCTTACGCCCC) and FhuEcatR (CCTCCTCCGGCATGAGCCTGACGACAACATAAACCAAGAGATTTCAAA-TGCTGGGCCAACTTTTGGCGAA). The following PCR conditions were used: (1) 98 °C for 30 s; (2) 30 cycles of 98 °C for 10 s, 70 °C for 20 s and 72 °C for 3 s; and (3) 72 °C for 5 min. Amplification was performed on 4 ng of pKD3 plasmid using Q5 High-Fidelity 2× Master Mix (New England Biolabs). The PCR product was digested for 1 h with the restriction enzymes DpnI and ClaI at 37 °C and then the PCR product was run on a 1% agarose gel. The PCR product was extracted using a QIAquick Gel Extraction kit (Qiagen) and then dialysed for 4h with TE buffer. A total of 1.5 µl of dialysed PCR product was used to transform the electrocompetent  $\Delta fepC$ -pkD46 or  $\Delta fepA$ -pkD46 cells. After 2 h of recovery in SOC medium with 1 mM arabinose at 37 °C, the transformants was plated on LB with 50 mg ml<sup>-1</sup> kanamycin and chloramphenicol. Transformants were confirmed to be  $\Delta fhuE$  with Eton Bioscience sequencing of the chloramphenical cassette.

Creation of  $\Delta fepA\Delta fhuA$ . Creation was done as for  $\Delta fepA\Delta fhuE$ , except that the chloramphenicol resistance cassette was amplified from pKD3 (ref. \*\*s\*) using FhuAcatF (ATCATTCTGGTTTACGTTATCACTTT ACATCAGAGATATACCAATGAATGGCGCGCCTTACGCCCCAATGGCGCGCCTTACGCCCC) and FhuAcatR (GCACGGAAATCCGTGCCCCAAAAGAGAAATTAGAAACGGAAGGTTGCGGTCTGGGCCAACTTTTTGGCGAACTGGGCCAACTTTTTGGCGAACTGGGCCAACTTTTTGGCGAAC) custom primers.

Penicillium sp. str. 12 genome sequencing, assembly and annotation. gDNA was extracted from Penicillium sp. str. 12 using the gDNA extraction protocol described above. High molecular weight DNA (average 16 kilobases) was sequenced on an Oxford Nanopore MinION with a R.9.5 flow cell using 1D² sequencing adaptors from kit SQK-LSK308 (Oxford Nanopore Technologies). Raw data were base called using guppy 3.3.0 (Oxford Nanopore Technologies) (guppy\_basecaller -config dna\_r9.5\_450bps.cfg -fast5\_out) for 1D base calls and these were used to also obtain higher accuracy 1D² base calls (guppy\_basecaller\_1d2 -i 1Dbasecall/ workspace/ -config dba\_r9.5\_450bps\_1d2\_raw.cfg -index\_file 1Dbasecall/ sequencing\_summary.txt). These reads were assembled by canu 1.8 (ref. \*9) and polished by racon 1.4.3 (ref. \*9) four times and by pilon 1.23 (ref. \*9) once. The final assembly is 38 Mbp and consists of 52 contigs.

Penicillium sp. str. 12 genome annotations were obtained by combining genomic and transcriptomic information from RNA-seq. To obtain the gene expression profile of Penicillium sp. str. 12, approximately 700,000 WT Penicillium sp. str. 12 spores were inoculated in triplicate on 10% CCA pH7 in standard petri dishes. After 3 days, the biofilms were collected for RNA extraction and washed with 1 ml of RNAprotect. RNA was extracted and RNA-seq libraries were prepared as described above with the following modification: ribosomal RNA depletion was performed using a RiboMinus Eukaryote kit v1, and RNA was recovered by ethanol precipitation. After sequencing, the RNA-seq reads from these Penicillium sp. str. 12 alone cultures were concatenated with RNA-seq reads from the previously described E. coli-Penicillium sp. str. 12 co-culture conditions that uniquely mapped to a single location on the Penicillium sp. str. 12 genome. The full set of transcriptomic reads was then used as input into the FunGAP annotation pipeline and 77 million of these reads were mapped 92. This pipeline predicted 13,261 protein-coding genes in the Penicillium sp. str. 12 genome. Interproscan<sup>93</sup> was used within the FunGAP pipeline for function prediction of genes. This Whole Genome Shotgun project has been deposited at DDBJ/ENA/GenBank under the accession JAASRZ000000000. The version described in this paper is version JAASRZ010000000.

Creation and confirmation of *Penicillium* sp. str. 12 *laeA* deletion mutant. The deletion cassette design strategy involved knocking out *laeA* in *Penicillium* sp. str. 12, whereby the isolate was first screened for hygromycin and phleomycin resistance. *Penicillium* sp. str. 12 showed a confirmed sensitivity to both antibiotics. A three-round PCR deletion strategy was used to replace the *laeA* open reading frame (ORF) with the *hph* gene, whose expression confers selection on hygromycin<sup>94</sup>. A schematic representation of the *laeA* gene replacement with the *hph* gene is depicted in Supplementary Fig. 3. The deletion cassette (5'flank- hph- 3'flank) was constructed using three sequential PCR reactions. In the first PCR round, about 1 kilobase of the genome sequence flanking either the 5' or 3' end of the *laeA* ORF was amplified using the primer sets P12\_KOlaeA\_5'F (CTCCGTTGGGCCCTCAC) and 5'R

(GCAATTTAACTGTGATAAACTACCGCATTAAAGCTGTTGATATCGGC AATCAATCAATG) or P12\_KOlaeA\_3'F (GGTGGGCCCTTGACATGTGCAGCC GGTGGAGCGGCCTGGTGAATCCTACCCACATGG) and 3'R (CGTTGG GAGGAAAAGCTTCTGCG), respectively. The hph gene was amplified from plasmid pUCH2-8 using primers hph\_F (AGCTTTAATGCGGTAGTTTATCA CAG) and hph\_R (CTCCACCGGCTGCACATGTC). A second PCR reaction was performed to assemble the three individual fragments from the first round of PCR by homologous recombination. The deletion cassettes were finally amplified using the nested primer set P12\_KOlaeA\_NestedF (CAGACGGTCCCGCATCCCG) and P12\_KOlaeA\_NestedR (GGTCCAGGTGCAGTAGTACTG).

To generate the deletion strains, a protoplast-mediated transformation protocol was employed. Briefly, 109 fresh spores were cultured in 500 ml of liquid minimal medium for 12 h at 25 °C and 280 r.p.m. Newly born hyphae were collected by centrifugation at 8,000 r.p.m. for 15 min and hydrolysed in a mixture of 30 mg Lysing Enzyme from Trichoderma (Sigma-Aldrich) and 20 mg Yatalase (Fisher Scientific) in 10 ml of osmotic medium (1.2 M MgSO<sub>4</sub>, 10 mM NaPB, pH 5.8). The quality of the protoplasts was monitored under the microscope after 4h of shaking at 28°C and 80 r.p.m. The protoplast mixture was later overlaid with 10 ml of trapping buffer (0.6 M sorbitol, 100 mM Tris-HCl pH 7.0) and centrifuged for 15 min at 4 °C and 5,000 r.p.m. Protoplasts were collected from the interface, overlaid with an equal volume of STC (1.2 M sorbitol, 10 mM Tris-HCL pH 7.5,10 mM CaCl<sub>2</sub>) and decanted by centrifugation at 6,000 r.p.m. for 8 min. The protoplast pellet was resuspended in 500 µl STC and used for transformation. After 5 days of incubation at 25 °C, colonies grown on stabilized minimal medium plates supplemented with hygromycin were subjected to a second round of selection on hygromycin plates. In total, 25 hygromycin-resistant transformants were isolated after a rapid screening procedure on stabilized minimal medium supplemented with hygromycin. Single-spored transformants were later tested for proper homologous recombination at the ORF locus by PCR and Southern blot analysis.

The correct replacement of  $\mathit{laeA}$  with the  $\mathit{hph}$  gene was first verified by PCR analysis of gDNA from the transformant strains using the primer set P12\_laeA\_F (CACAATGGCTGAACACTCTCGG) and P12\_laeA\_R (GGGATATGGAGCATCGAAGTTGC) that amplify the  $\mathit{laeA}$  ORF. About 12% (3 out of 25) of the monoconidial lines generated from primary transformants of  $\mathit{Penicillium}$  sp. str. 12 were PCR-positive for the absence of the  $\mathit{laeA}$  ORF. The positive deletion strains were further checked for a single insertion of the deletion cassette by Southern blot analysis and revealed single-site integration of the deletion cassette in one transformant (Supplementary Fig. 3). Probes corresponding to the 5' and 3' flanks of the  $\mathit{laeA}$  gene in each strain were labelled using  $[\alpha 32P]$  dCTP (PerkinElmer) following the manufacturer's instructions.

RNA-seq analysis of WT and  $\Delta laeA$  Penicillium sp. str. 12. To characterize the effect of the laeA deletion on the Penicillium sp. str. 12 gene expression profile, we performed RNA-seq analysis for  $\Delta laeA$  Penicillium sp. str. 12. As for WT Penicillium sp. str. 12, 700,000  $\Delta laeA$  Penicillium sp. str. 12 spores were inoculated in triplicate (three distinct samples) on 10% CCA pH7 in standard petri dishes, and biofilms were collected after 3 days. Collection, RNA extraction and library preparation were performed identically to that for WT Penicillium sp. str. 12. Then, Penicillium sp. str. 12 and  $\Delta laeA$  differential expression analysis was performed as described for E. coli-Penicillium sp. str. 12 above. To look for enrichment of functions in the set of differentially expressed genes, we input the protein sequences of the genes into the gene-list enrichment function of KOBAS 3.0 (ref.  $^{95}$ ). Sequences were searched against the GO database $^{96,97}$  using A. fumigatus as reference for GO assignment before conducting a hypergeometric test with Benjamini-Hochberg correction. Functions with a corrected P<0.05 were considered enriched.

WT and Δ*laeA Penicillium* sp. str. 12 growth assays. For radial growth assays, 2,000 WT or Δ*laeA Penicillium* sp. str. 12 fungal spores were inoculated as spots in triplicate on 10% CCA pH7 either alone or with 20,000 *E. coli* cells. The radius of fungal growth was measured after 7 days. For spore counting assays, we aimed to inoculate 6,000 WT or Δ*laeA Penicillium* sp. str. 12 fungal spores per well on 10% CCA pH7 in a 96-well plate either alone or co-inoculated with 60,000 *E. coli* cells. Each assay was done in triplicate. After 7 days of growth, the entire well was collected and homogenized in 1× PBS–Tween 0.05% before dilution and plating on PCAMS with 50μg ml<sup>-1</sup> chloramphenicol (for fungal spore counts).

Availability of biological materials. All unique materials, including the described fungal strains isolated from cheese, the *P. psychrophila* JB418 strain and the RB-TnSeq library, the *Penicillium* sp. str. 12 *laeA* deletion mutant and the *E. coli* siderophore-uptake double mutants, are readily available from the authors upon request. The *E. coli* RB-TnSeq library and Keio strains can be requested from the groups that created these resources (PMID references are provided in Supplementary Table 19).

**Reporting Summary.** Further information on research design is available in the Nature Research Reporting Summary linked to this article.

#### Data availability

Sequence data that support the findings of this study (RB-TnSeq and RNA-seq) have been deposited in the NCBI SRA database with SRA accession codes SRR11514793-SRR11514872 and BioProject code PRJNA624168. MS data are available in the MassIVE database under accession numbers MSV000085070 and MSV000085054. The GNPS molecular network is available at https://gnps.ucsd. edu/ProteoSAFe/status.jsp?task=464b331ef9d54de9957d23b4f9b9db14. The E. coli annotation database used for GO functional enrichment is available at http://bioconductor.org/packages/release/data/annotation/html/org.EcK12.eg.db. html. The Whole Genome Shotgun project for *Penicillium* sp. str. 12, including reads, genome assembly and annotation has been deposited at DDBJ/ENA/ GenBank under the accession JAASRZ000000000 in BioProject PRJNA612335 (BioSample SAMN14369290 and SRA SRR11536435). In addition to these sources, the data used to create Figs. 2, 3, 5 and 6 are available in the Supplementary Tables provided with the paper. Uncropped Southern blots associated with Supplementary Fig. 3 are provided with the manuscript as Supplementary Data. Source data are provided with this paper.

# Code availability

The R scripts developed for processing RB-TnSeq data described in this manuscript are available at https://github.com/DuttonLab/RB-TnSeq-Microbial-interactions along with usage instructions. The perl scripts needed for initial processing of RB-TnSeq data published in Wetmore et al. 18 are available at https://bitbucket.org/berkeleylab/feba/src/master/.

Received: 30 March 2020; Accepted: 16 September 2020; Published online: 02 November 2020

#### References

- Laforest-Lapointe, I. & Arrieta, M.-C. Microbial eukaryotes: a missing link in gut microbiome studies. mSystems 3, e00201-17 (2018).
- Huseyin, C. E., O'Toole, P. W., Cotter, P. D. & Scanlan, P. D. Forgotten fungi—the gut mycobiome in human health and disease. FEMS Microbiol. Rev. 41, 479–511 (2017).
- Bergelson, J., Mittelstrass, J. & Horton, M. W. Characterizing both bacteria and fungi improves understanding of the *Arabidopsis* root microbiome. Sci. Rep. 9, 24 (2019).
- Huffnagle, G. B. & Noverr, M. C. The emerging world of the fungal microbiome. *Trends Microbiol.* 21, 334–341 (2013).
- Bradford, L. L. & Ravel, J. The vaginal mycobiome: a contemporary perspective on fungi in women's health and diseases. Virulence 8, 342–351 (2017).
- de Phillips, F., Laiola, M., Blaiotta, G. & Ercolini, D. Different amplicon targets for sequencing-based studies of fungal diversity. *Appl. Environ. Microbiol.* 83, e00905-17 (2017).
- Jiang, T. T. et al. Commensal fungi recapitulate the protective benefits of intestinal bacteria. Cell Host Microbe 22, 809–816 (2017).
- Wagg, C., Schlaeppi, K., Banerjee, S., Kuramae, E. E. & van der Heijden, M. G. A. Fungal-bacterial diversity and microbiome complexity predict ecosystem functioning. *Nat. Commun.* 10, 4841 (2019).
- Durán, P. et al. Microbial interkingdom interactions in roots promote *Arabidopsis* survival. Cell 175, 973–983 (2018).
- Tourneroche, A. et al. Bacterial-fungal interactions in the kelp endomicrobiota drive autoinducer-2 quorum sensing. Front. Microbiol. 10, 1693 (2019).
- Lindsay, A. K. & Hogan, D. A. Candida albicans: molecular interactions with Pseudomonas aeruginosa and Staphylococcus aureus. Fungal Biol. Rev. 28, 85–96 (2014).
- Xu, X.-L. et al. Bacterial peptidoglycan triggers Candida albicans hyphal growth by directly activating the adenylyl cyclase Cyr1p. Cell Host Microbe 4, 28–39 (2008).
- Spraker, J. E. et al. Conserved responses in a war of small molecules between a plant-pathogenic bacterium and fungi. mBio 9, e00820-18 (2018).
- Khalid, S. et al. NRPS-derived isoquinolines and lipopetides mediate antagonism between plant pathogenic fungi and bacteria. ACS Chem. Biol. 13, 171–179 (2018).
- Wolfe, B. E., Button, J. E., Santarelli, M. & Dutton, R. J. Cheese rind communities provide tractable systems for in situ and in vitro studies of microbial diversity. *Cell* 158, 422–433 (2014).
- Morin, M., Pierce, E. C. & Dutton, R. J. Changes in the genetic requirements for microbial interactions with increasing community complexity. eLife 7, e37072 (2018).
- Zhang, Y., Kastman, E. K., Guasto, J. S. & Wolfe, B. E. Fungal networks shape dynamics of bacterial dispersal and community assembly in cheese rind microbiomes. *Nat. Commun.* 9, 336 (2018).
- Wetmore, K. M. et al. Rapid quantification of mutant fitness in diverse bacteria by sequencing randomly bar-coded transposons. mBio 6, e00306-15 (2015).

- Hallen-Adams, H. E. & Suhr, M. J. Fungi in the healthy human gastrointestinal tract. *Virulence* 8, 352–358 (2017).
- Frac, M., Hannula, S. E., Bełka, M. & Jędryczka, M. Fungal biodiversity and their role in soil health. Front. Microbiol. 9, 707 (2018).
- Dukare, A. S. et al. Exploitation of microbial antagonists for the control of postharvest diseases of fruits: a review. Crit. Rev. Food Sci. Nutr. 59, 1498–1513 (2019).
- Richards, T. A., Jones, M. D. M., Leonard, G. & Bass, D. Marine fungi: their ecology and molecular diversity. *Ann. Rev. Mar. Sci.* 4, 495–522 (2012).
- Choi, K.-H., Lee, H., Lee, S., Kim, S. & Yoon, Y. Cheese microbial risk assessments—a review. Asian-Australas. J. Anim. Sci. 29, 307–314 (2016).
- 24. Perrin, F. et al. Quantitative risk assessment of haemolytic and uremic syndrome linked to O157:H7 and non-O157:H7 shiga-toxin producing Escherichia coli strains in raw milk soft cheeses: quantitative risk assessment of HUS linked to pathogenic STEC in cheese. Risk Anal. 35, 109–128 (2015).
- Cosetta, C. M. & Wolfe, B. E. Deconstructing and reconstructing cheese rind microbiomes for experiments in microbial ecology and evolution. Curr. Protoc. Microbiol. 56, e95 (2020).
- Calvo, A. M., Wilson, R. A., Bok, J. W. & Keller, N. P. Relationship between secondary metabolism and fungal development. *Microbiol. Mol. Biol. Rev.* 66, 447–459 (2002).
- Nonejuie, P., Burkart, M., Pogliano, K. & Pogliano, J. Bacterial cytological profiling rapidly identifies the cellular pathways targeted by antibacterial molecules. *Proc. Natl Acad. Sci. USA* 110, 16169–16174 (2013).
- Bok, J. W. & Keller, N. P. LaeA, a regulator of secondary metabolism in Aspergillus spp. Eukaryot. Cell 3, 527–535 (2004).
- Kosalková, K. et al. The global regulator LaeA controls penicillin biosynthesis, pigmentation and sporulation, but not roquefortine C synthesis in *Penicillium chrysogenum*. *Biochimie* 91, 214–225 (2009).
- Laich, F., Fierro, F. & Martín, J. F. Production of penicillin by fungi growing on food products: identification of a complete penicillin gene cluster in Penicillium griseofulvum and a truncated cluster in Penicillium verrucosum. Appl. Environ. Microbiol. 68, 1211–1219 (2002).
- Streit, W. R. & Entcheva, P. Biotin in microbes, the genes involved in its biosynthesis, its biochemical role and perspectives for biotechnological production. *Appl. Microbiol. Biotechnol.* 61, 21–31 (2003).
- 32. Kastman, E. K. et al. Biotic interactions shape the ecological distributions of *Staphylococcus* species. *mBio* 7, e01157-16 (2016).
- Bonham, K. S., Wolfe, B. E. & Dutton, R. J. Extensive horizontal gene transfer in cheese-associated bacteria. eLife 6, e22144 (2017).
- Dean, C. R. & Poole, K. Expression of the ferric enterobactin receptor (PfeA) of *Pseudomonas aeruginosa*: involvement of a two-component regulatory system. *Mol. Microbiol.* 8, 1095–1103 (1993).
- Schalk, I. J., Rigouin, C. & Godet, J. An overview of siderophore biosynthesis among fluorescent Pseudomonads and new insights into their complex cellular organization. *Environ. Microbiol.* 22, 1447–1466 (2020).
- Fecker, L. & Braun, V. Cloning and expression of the *fhu* genes involved in iron(III)-hydroxamate uptake by *Escherichia coli. J. Bacteriol.* 156, 1301–1314 (1983).
- Sauer, M., Hantke, K. & Braun, V. Ferric-coprogen receptor FhuE of *Escherichia coli*: processing and sequence common to all TonB-dependent outer membrane receptor proteins. *J. Bacteriol.* 169, 2044–2049 (1987).
- Blin, K. et al. antiSMASH 5.0: updates to the secondary metabolite genome mining pipeline. *Nucleic Acids Res.* 47, W81–W87 (2019).
- Triana, S. et al. Draft genome sequence of the animal and human pathogen malassezia pachydermatis strain CBS 1879. Genome Announc. 3, e01197-15 (2015).
- Sarkar, S. K., Chowdhury, C. & Ghosh, A. S. Deletion of penicillin-binding protein 5 (PBP5) sensitises *Escherichia coli* cells to β-lactam agents. *Int. J. Antimicrob. Agents* 35, 244–249 (2010).
- Perrin, R. M. et al. Transcriptional regulation of chemical diversity in *Aspergillus fumigatus* by LaeA. PLoS Pathog. 3, e50 (2007).
- Haas, H. Fungal siderophore metabolism with a focus on Aspergillus fumigatus. Nat. Prod. Rep. 31, 1266–1276 (2014).
- Luckner, M. [On the synthesis of quinoline alkaloids in plants. 2.
   Fermentativ conversion of the penicillin alkaloids cyclopenin and cyclopenol to viridicatin and viridicatol]. Eur. J. Biochem. 2, 74–78 (1967).
- Peters, B. M., Jabra-Rizk, M. A., O'May, G. A., Costerton, J. W. & Shirtliff, M. E. Polymicrobial interactions: impact on pathogenesis and human disease. *Clin. Microbiol. Rev.* 25, 193–213 (2012).
- Scherlach, K., Graupner, K. & Hertweck, C. Molecular bacteria–fungi interactions: effects on environment, food, and medicine. *Annu. Rev. Microbiol.* 67, 375–397 (2013).
- de Boer, W., Folman, L. B., Summerbell, R. C. & Boddy, L. Living in a fungal world: impact of fungi on soil bacterial niche development. FEMS Microbiol. Rev. 29, 795–811 (2005).
- 47. Johansson, J. F., Paul, L. R. & Finlay, R. D. Microbial interactions in the mycorrhizosphere and their significance for sustainable agriculture. *FEMS Microbiol. Ecol.* **48**, 1–13 (2004).

- Tarkka, M. T., Sarniguet, A. & Frey-Klett, P. Inter-kingdom encounters: recent advances in molecular bacterium–fungus interactions. *Curr. Genet.* 55, 233–243 (2009).
- Taga, M. E. & Walker, G. C. Sinorhizobium meliloti requires a cobalamindependent ribonucleotide reductase for symbiosis with its plant host. Mol. Plant. Microbe Interact. 23, 1643–1654 (2010).
- Deveau, A. et al. Role of fungal trehalose and bacterial thiamine in the improved survival and growth of the ectomycorrhizal fungus *Laccaria* bicolor S238N and the helper bacterium *Pseudomonas fluorescens* BBc6R8. Environ. Microbiol. Rep. 2, 560–568 (2010).
- Hantke, K. Identification of an iron uptake system specific for coprogen and rhodotorulic acid in *Escherichia coli* K12. Mol. Gen. Genet. 191, 301–306 (1983)
- Arias, A. A. et al. Growth of desferrioxamine-deficient Streptomyces mutants through xenosiderophore piracy of airborne fungal contaminations. FEMS Microbiol. Rev. 91, fiv080 (2015).
- Haas, H., Eisendle, M. & Turgeon, B. G. Siderophores in fungal physiology and virulence. *Annu. Rev. Phytopathol.* 46, 149–187 (2008).
- Park, M., Cho, Y.-J., Lee, Y. W. & Jung, W. H. Understanding the mechanism of action of the anti-dandruff agent zinc pyrithione against Malassezia restricta. Sci. Rep. 8, 12086 (2018).
- Gründlinger, M. et al. Fungal siderophore biosynthesis is partially localized in peroxisomes. Mol. Microbiol. 88, 862–875 (2013).
- Heymann, P., Ernst, J. F. & Winkelmann, G. A gene of the major facilitator superfamily encodes a transporter for enterobactin (Enb1p) in Saccharomyces cerevisiae. Biometals 13, 65–72 (2000).
- Sass, G. et al. Studies of *Pseudomonas aeruginosa* mutants indicate pyoverdine as the central factor in inhibition of *Aspergillus fumigatus* biofilm. *J. Bacteriol.* 200, e00345-17 (2017).
- Briard, B. et al. Pseudomonas aeruginosa manipulates redox and iron homeostasis of its microbiota partner Aspergillus fumigatus via phenazines. Sci. Rep. 5, 8220 (2015).
- Clancy, A. et al. Evidence for siderophore-dependent iron acquisition in group B streptococcus. Mol. Microbiol. 59, 707–721 (2006).
- Jin, B. et al. Iron acquisition systems for ferric hydroxamates, haemin and haemoglobin in *Listeria monocytogenes*. Mol. Microbiol. 59, 1185–1198 (2006).
- Mishra, R. P. N. et al. Staphylococcus aureus FhuD2 is involved in the early phase of staphylococcal dissemination and generates protective immunity in mice. J. Infect. Dis. 206, 1041–1049 (2012).
- Rocha, E. R. & Krykunivsky, A. S. Anaerobic utilization of Fe(III)-xenosiderophores among *Bacteroides* species and the distinct assimilation of Fe(III)-ferrichrome by *Bacteroides fragilis* within the genus. *MicrobiologyOpen* 6, e00479 (2017).
- Li, H. et al. The outer mucus layer hosts a distinct intestinal microbial niche. Nat. Commun. 6, 8292 (2015).
- Ong, S. A. & Neilands, J. B. Siderophores in microbially processed cheese. J. Agric. Food Chem. 27, 990–995 (1979).
- David, L. A. et al. Diet rapidly and reproducibly alters the human gut microbiome. *Nature* 505, 559–563 (2014).
- Rehner, S. A. & Samuels, G. J. Molecular systematics of the Hypocreales: a teleomorph gene phylogeny and the status of their anamorphs. *Can. J. Bot.* 73, 816–823 (1995).
- Glass, N. L. & Donaldson, G. C. Development of primer sets designed for use with the PCR to amplify conserved genes from filamentous ascomycetes. *Appl. Environ. Microbiol.* 61, 1323–1330 (1995).
- Ronquist, F. & Huelsenbeck, J. P. MrBayes 3: Bayesian phylogenetic inference under mixed models. *Bioinformatics* 19, 1572–1574 (2003).
- Dunnett, C. W. A multiple comparison procedure for comparing several treatments with a Control. *J. Am. Stat. Assoc.* 50, 1096–1121 (1955).
- Wickham, H. ggplot2: Elegant Graphics for Data Analysis (Springer Science+Business Media, 2009).
- Cleary, J. L., Luu, G. T., Pierce, E. C., Dutton, R. J. & Sanchez, L. M. BLANKA: an algorithm for blank subtraction in mass spectrometry of complex biological samples. *J. Am. Soc. Mass. Spectrom.* 30, 1426–1434 (2019).
- 72. Mohimani, H. et al. Dereplication of microbial metabolites through database search of mass spectra. *Nat. Commun.* **9**, 4035 (2018).
- Mohimani, H. et al. Dereplication of peptidic natural products through database search of mass spectra. Nat. Chem. Biol. 13, 30–37 (2017).
- Shannon, P. et al. Cytoscape: a software environment for integrated models of biomolecular interaction networks. Genome Res. 13, 2498–2504 (2003).
- Benjamini, Y. & Hochberg, Y. Controlling the false discovery rate: a practical and powerful approach to multiple testing. J. R. Stat. Soc. Ser. B Stat. Methodol. 57, 289–300 (1995).
- Tang, Y., Horikoshi, M. & Li, W. ggfortify: unified interface to visualize statistical result of popular R packages. R Journal 8, 474–485 (2016).

 Huerta-Cepas, J. et al. eggNOG 5.0: a hierarchical, functionally and phylogenetically annotated orthology resource based on 5090 organisms and 2502 viruses. *Nucleic Acids Res.* 47, D309–D314 (2019).

- Yu, G., Wang, L.-G., Han, Y. & He, Q.-Y. clusterProfiler: an R package for comparing biological themes among gene clusters. *OMICS* 16, 284–287 (2012).
- 79. Carlson, M. org.EcK12.eg.db: Genome wide annotation for *E. coli* strain K12. R package version 3.8.2. (Bioconductor, 2019).
- Carlson, M. & Pagès, H. AnnotationForge: tools for building SQLite-based annotation data packages. R package version 1.26.0 (Bioconductor, 2019).
- Baba, T. et al. Construction of Escherichia coli K-12 in-frame, single-gene knockout mutants: the Keio collection. Mol. Syst. Biol. 2, 2006.0008 (2006).
- Schindelin, J. et al. Fiji: an open-source platform for biological-image analysis. Nat. Methods 9, 676–682 (2012).
- Schwyn, B. & Neilands, J. B. Universal chemical assay for the detection and determination of siderophores. *Anal. Biochem.* 160, 47–56 (1987).
- Payne, S. M. Detection, isolation, and characterization of siderophores. *Methods Enzymol.* 235, 329–344 (1994).
- 85. Grenier, F., Matteau, D., Baby, V. & Rodrigue, S. Complete genome sequence of *Escherichia coli* BW25113. *Genome Announc.* 2, e01038-14 (2014).
- Lawrence, M. et al. Software for computing and annotating genomic ranges. PLoS Comput. Biol. 9, e1003118 (2013).
- Love, M. I., Huber, W. & Anders, S. Moderated estimation of fold change and dispersion for RNA-seq data with DESeq2. *Genome Biol.* 15, 550 (2014).
- Datsenko, K. A. & Wanner, B. L. One-step inactivation of chromosomal genes in *Escherichia coli* K-12 using PCR products. *Proc. Natl Acad. Sci.* USA 97, 6640-6645 (2000).
- Koren, S. et al. Canu: scalable and accurate long-read assembly via adaptive k-mer weighting and repeat separation. *Genome Res.* 27, 722–736 (2017).
- Vaser, R., Sović, I., Nagarajan, N. & Šikić, M. Fast and accurate de novo genome assembly from long uncorrected reads. *Genome Res.* 27, 737–746 (2017).
- Walker, B. J. et al. Pilon: an integrated tool for comprehensive microbial variant detection and genome assembly improvement. PLoS ONE 9, e112963 (2014).
- Min, B., Grigoriev, I. V. & Choi, I.-G. FunGAP: fungal genome annotation pipeline using evidence-based gene model evaluation. *Bioinformatics* 33, 2936–2937 (2017).
- 93. Jones, P. et al. InterProScan 5: genome-scale protein function classification. *Bioinformatics* **30**, 1236–1240 (2014).
- Lim, F. Y., Sanchez, J. F., Wang, C. C. C. & Keller, N. P. Toward awakening cryptic secondary metabolite gene clusters in filamentous fungi. *Methods Enzymol.* 517, 303–324 (2012).
- Xie, C. et al. KOBAS 2.0: a web server for annotation and identification of enriched pathways and diseases. *Nucleic Acids Res.* 39, W316–W322 (2011).
- The Gene Ontology Consortium. The Gene Ontology Resource: 20 years and still GOing strong. Nucleic Acids Res. 47, D330–D338 (2019).
- Ashburner, M. et al. Gene Ontology: tool for the unification of biology. Nat. Genet. 25, 25–29 (2000).
- 98. Jukes, T. H. & Cantor, C. R. in Mammalian Protein Metabolism Vol. 3 (ed. Munro, H. N.) 21–132 (Academic Press, 1969).
- Conway, J. R., Lex, A. & Gehlenborg, N. UpSetR: an R package for the visualization of intersecting sets and their properties. *Bioinformatics* 33, 2938–2940 (2017).
- Patti, G. J. et al. A view from above: cloud plots to visualize global metabolomic data. Anal. Chem. 85, 798–804 (2013).

#### Acknowledgements

The authors would like to thank the following people and groups: the Arkin Lab and the Deutschbauer Lab at UC Berkeley for the E. coli Keio\_ML9 RB-TnSeq library; K. Jepsen at the IGM Genomics Center at the University of California, San Diego for assistance with sequencing; S. Kryazhimskiy (UCSD) for his input on RB-TnSeq data processing; C. Dinh (UCSD) for assistance with fungal genome assembly; W. Bushnell (UCSD) for assistance with fitness validation experiments; S. Beyhan (ICVI) for advice on fungal genome annotation; L. Marotz (UCSD) for assistance with non-cheese yeasts; and members of the Dutton Lab, especially B. Anderson and C. Saak, for constructive comments on the manuscript. This work was supported by the National Institutes of Health grant nos. T32-AT007533 (to J.C.L.) and F31-AT010418 (to J.C.L.), the National Institutes of Health grant no. R01-AI117712 (to R.B.L), National Science Foundation grant no. MCB-1817955 (to L.M.S.), National Science Foundation grant no. MCB-1817887 (to R.J.D. and L.M.S.), National Science Foundation grant no. MCB-1715553 (to B.E.W.), the UCSD Center for Microbiome Innovation (to E.C.P.), the UCSD Ruth Stern Award (to E.C.P.), NIH Institutional Training grant no. 5 T32 GM 7240-40 (to E.C.P.) and the National Institutes of Health grant no. R01GM112739-01 (to N.P.K.).

# **Author contributions**

R.J.D., L.M.S. and B.E.W. conceptualized the study. E.C.P., M.M., J.T., R.B.L. and J.C.L. performed the experiments. The R data processing pipeline was written by M.M. Data analyses were performed by E.C.P., J.C.L. and M.M. The article was written by E.C.P., M.M., L.M.S., J.C.L. and R.J.D. and revised with input from all authors. The figures were made by E.C.P. with input from L.M.S., J.C.L., R.J.D. and M.M., except for Fig. 4a and Extended Data Fig. 7 (R.B.L.), Fig. 6d (J.C.L.), Extended Data Figs. 1 and 2 (M.M.) and Supplementary Fig. 3 (J.T.). The study was supervised by R.J.D. and L.M.S.

#### **Competing interests**

The authors declare no competing interests.

# **Additional information**

**Extended data** is available for this paper at https://doi.org/10.1038/s41564-020-00800-z. **Supplementary information** is available for this paper at https://doi.org/10.1038/s41564-020-00800-z.

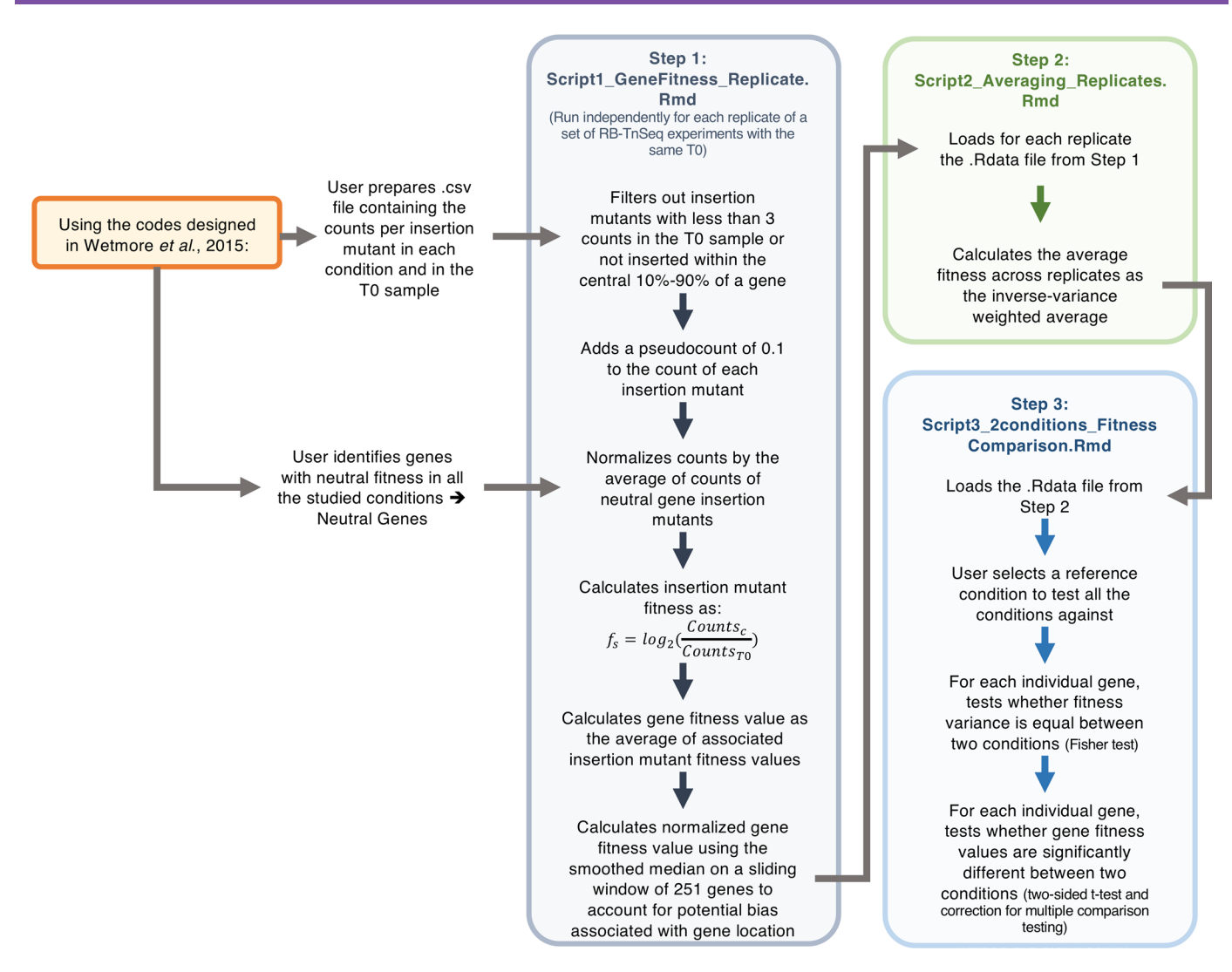
Correspondence and requests for materials should be addressed to R.J.D.

Peer review information Peer reviewer reports are available.

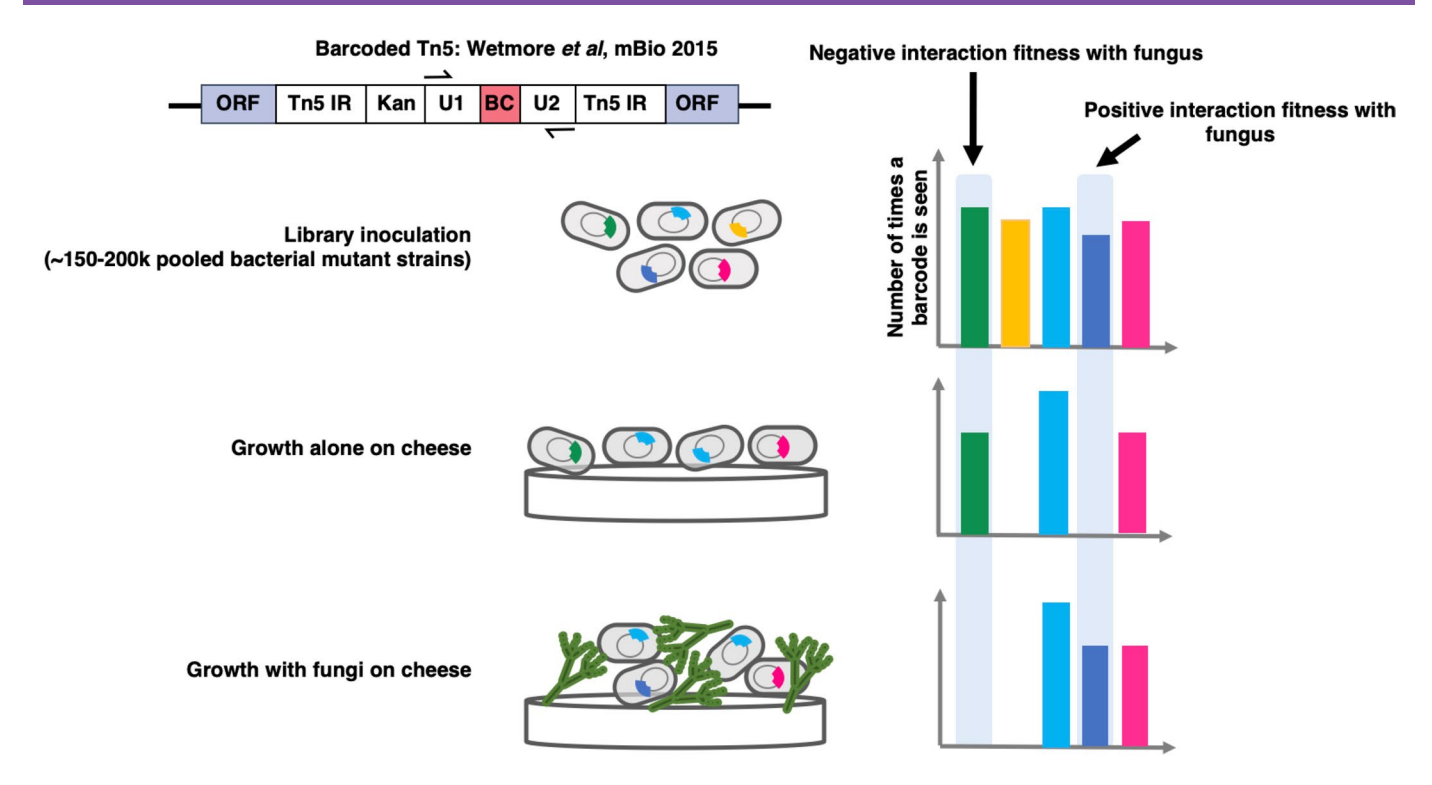
Reprints and permissions information is available at www.nature.com/reprints.

**Publisher's note** Springer Nature remains neutral with regard to jurisdictional claims in published maps and institutional affiliations.

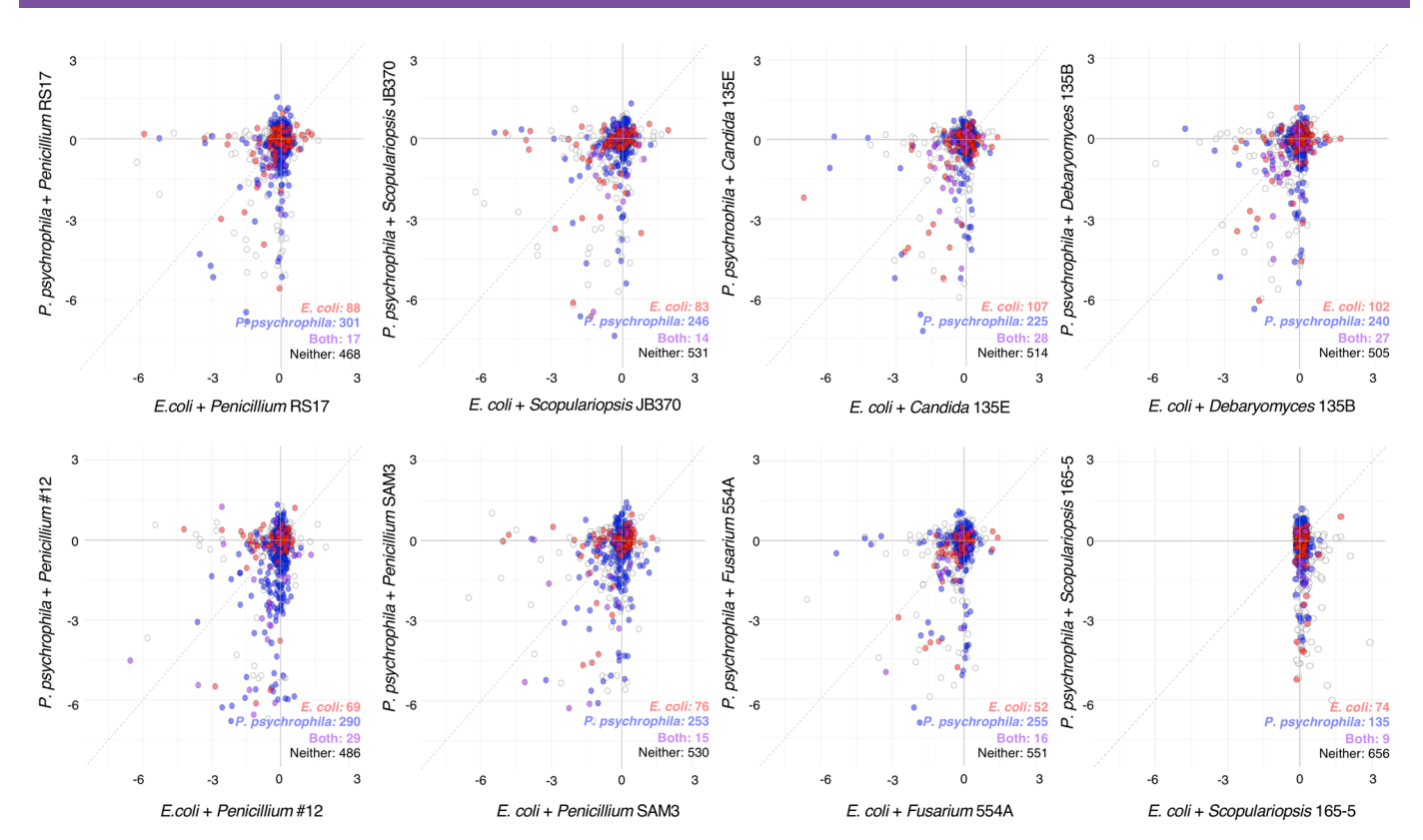
© The Author(s), under exclusive licence to Springer Nature Limited 2020



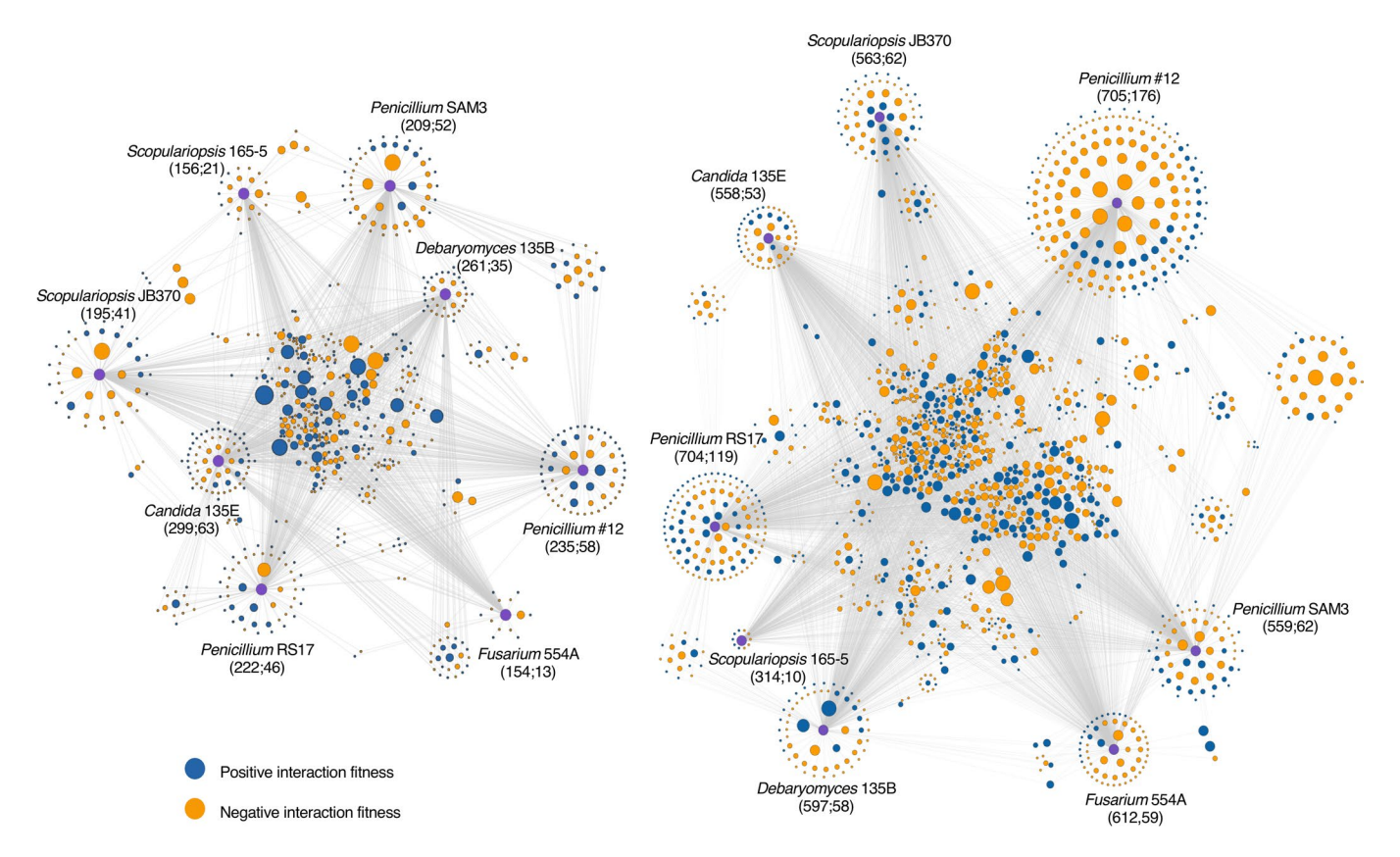
**Extended Data Fig. 1 | RB-TnSeq R data processing pipeline for gene fitness comparison across multiple conditions.** The pipeline is divided into three main scripts. Script 1 calculates the normalized gene fitness for each replicate of an RB-TnSeq experiment. This script has to be run for each replicate independently. Then, the .Rdata files from Script 1 are loaded in Script 2. Script 2 calculates for each RB-TnSeq condition the average gene fitness across replicates (inverse-variance weighted average). Finally, Script 3 compares gene fitness values of each RB-TnSeq condition against a chosen reference condition.



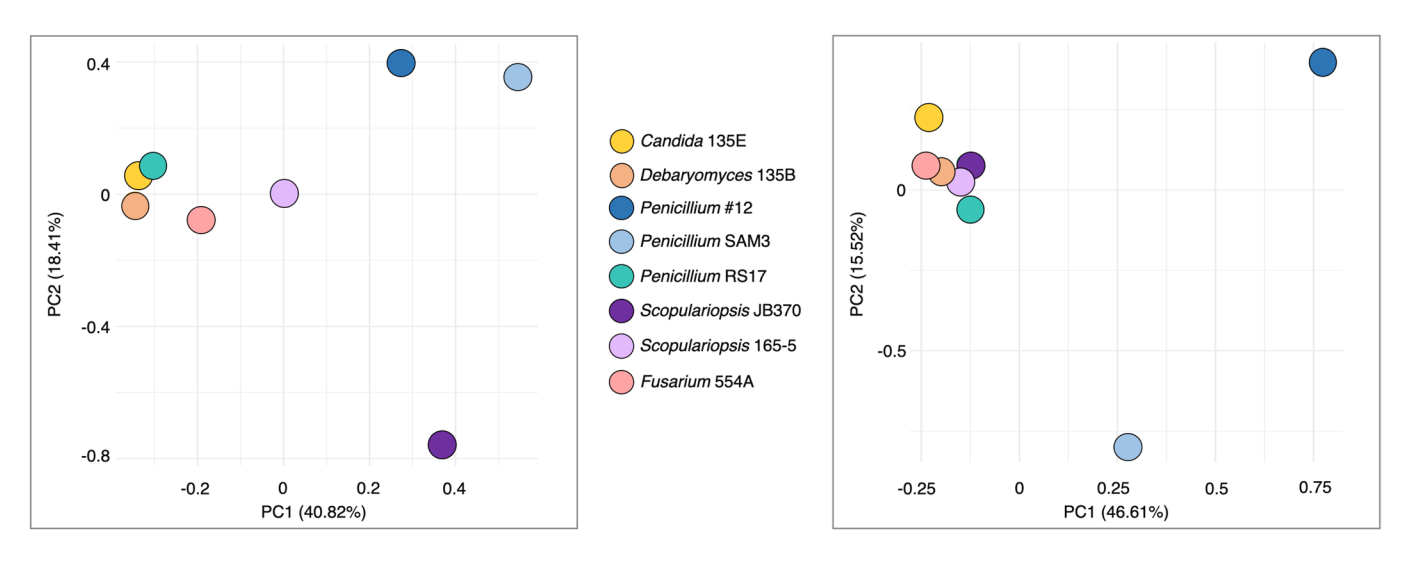
**Extended Data Fig. 2 | RB-TnSeq assay for fungal impacts on bacterial gene fitness.** Characterized pooled bacterial mutant libraries were grown in a biofilm either alone or with a fungal partner. After seven days of growth, mutant abundances were compared to the starting library abundances for each condition. Changes in barcode abundances were used to calculate gene fitness values. Genes with fitness values that differed significantly between co-culture and alone conditions (significant interaction fitness) were identified as potentially relevant to fungal interaction.



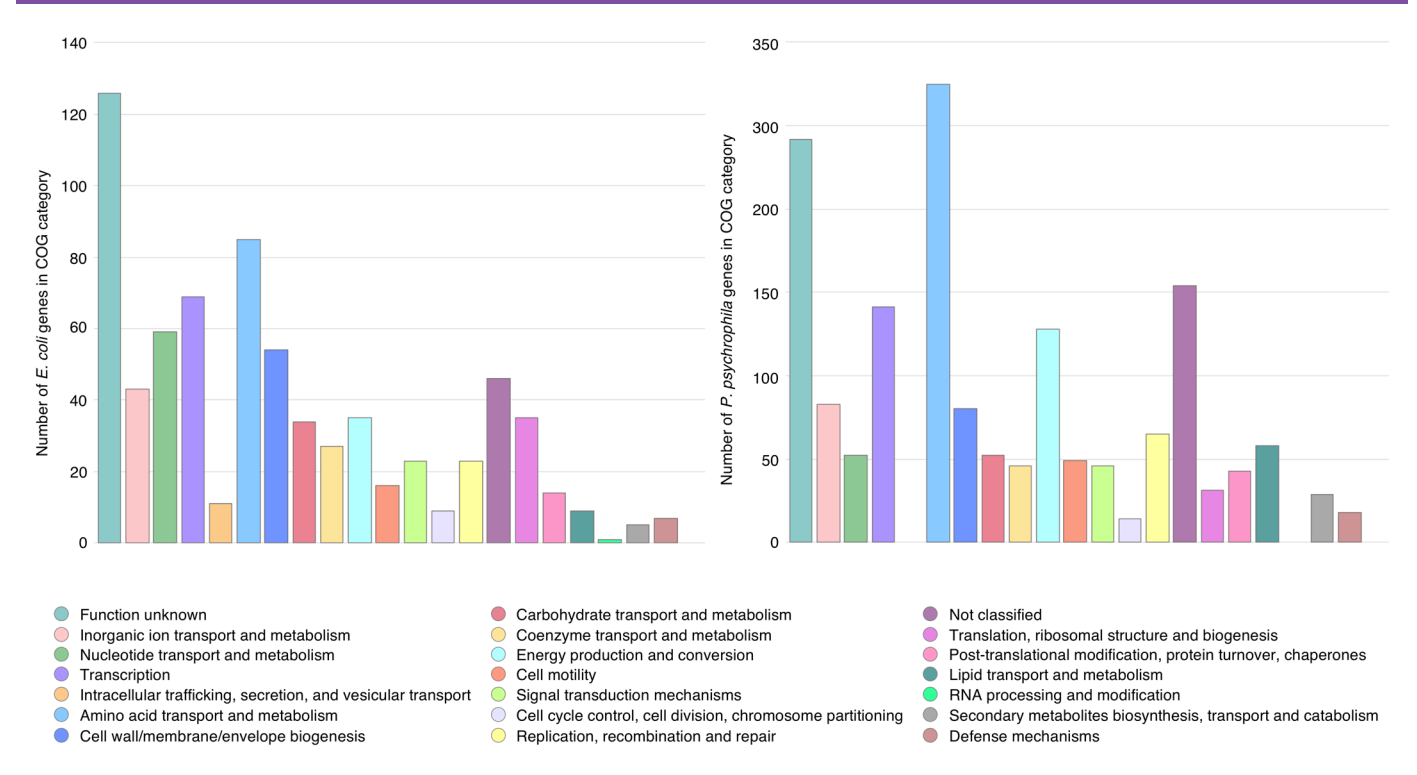
**Extended Data Fig. 3 | Comparison of** *E. coli* and *P. psychrophila* interaction fitness values for the 874 genes found in both bacteria. BLAST comparison (e-value cutoff of 1e-2) of protein sequences from *P. psychrophila* to those from *E. coli* and comparison of eggNOG gene assignments were used to find the best cross-species gene match for all genes with significant interaction fitness for at least one of the two bacterial species. A match was found for 874 genes. For each fungal condition, the fitness value of these genes with *E. coli* is on the x-axis and with *P. psychrophila* on the y-axis. In each condition, the genes are colored according to whether they have significant interaction fitness in the condition for *E. coli* (red), *P. psychrophila* (blue), both (purple), or neither (white).



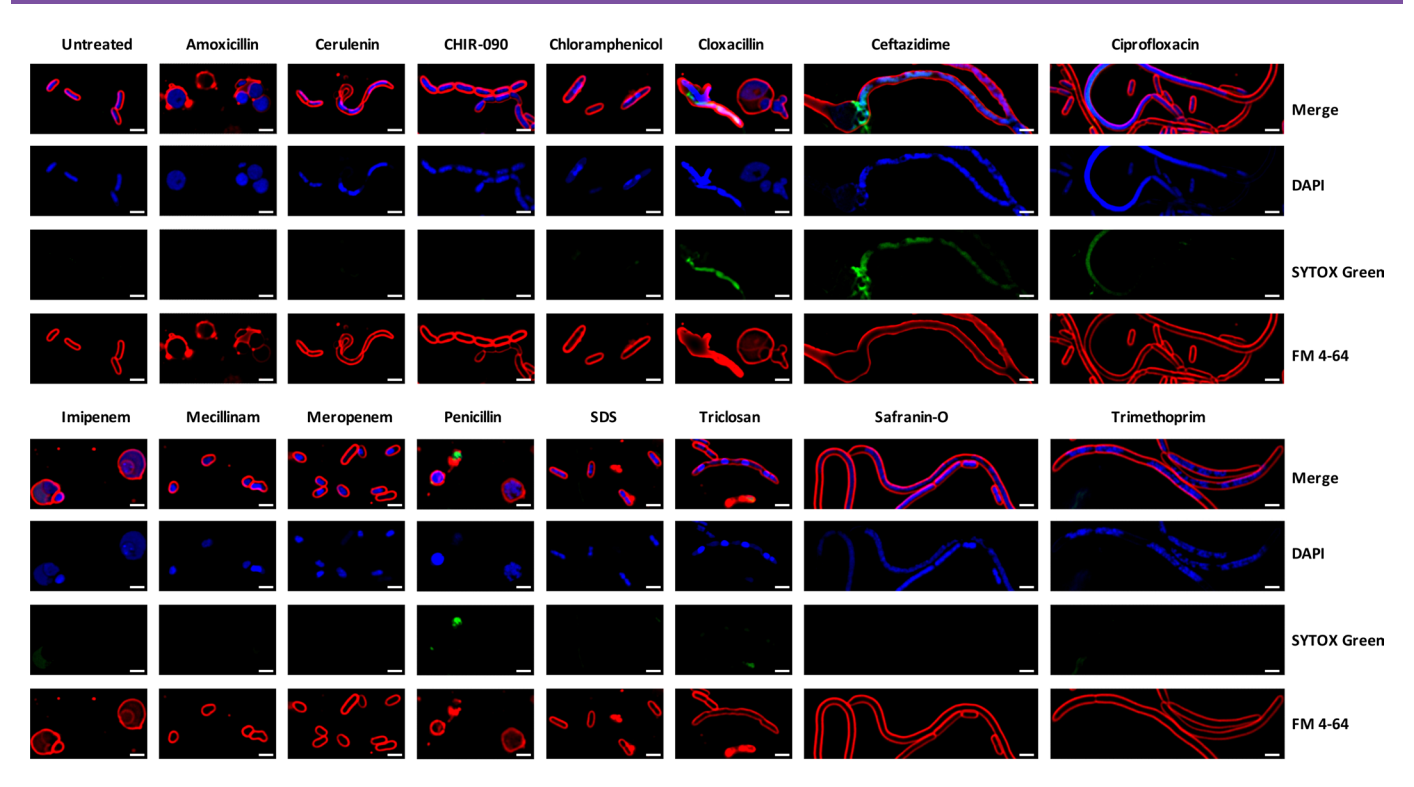
**Extended Data Fig. 4 | Network of** *E. coli* (left) or *P. psychrophila* (right) genes with positive and negative RB-TnSeq interaction fitness. Each purple node represents a fungal partner and is labeled as follows: fungal partner (number of genes with interaction fitness; number of genes with interaction fitness unique to this condition). Each blue or orange node represents a bacterial gene. Nodes are colored by whether the average interaction fitness is positive (blue) or negative (orange) as shown in the legend below and are sized by average strength of interaction fitness across partners.



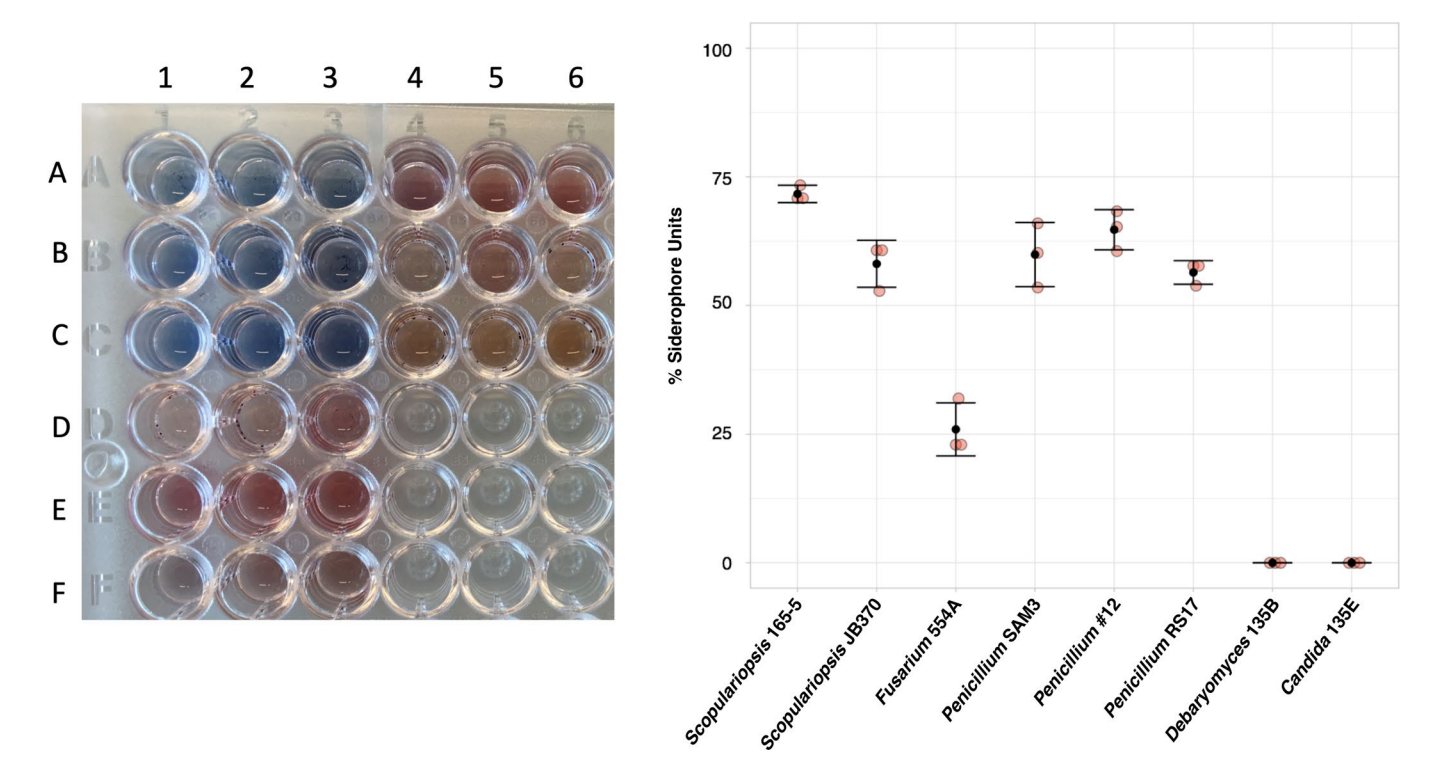
**Extended Data Fig. 5 | Principal Component Analysis of RB-TnSeq data.** Analysis was done on the fitness values in each fungal condition for all *E. coli* (left) or *P. psychrophila* (right) genes with an interaction fitness in at least one fungal condition. Each colored circle represents a fungal condition.



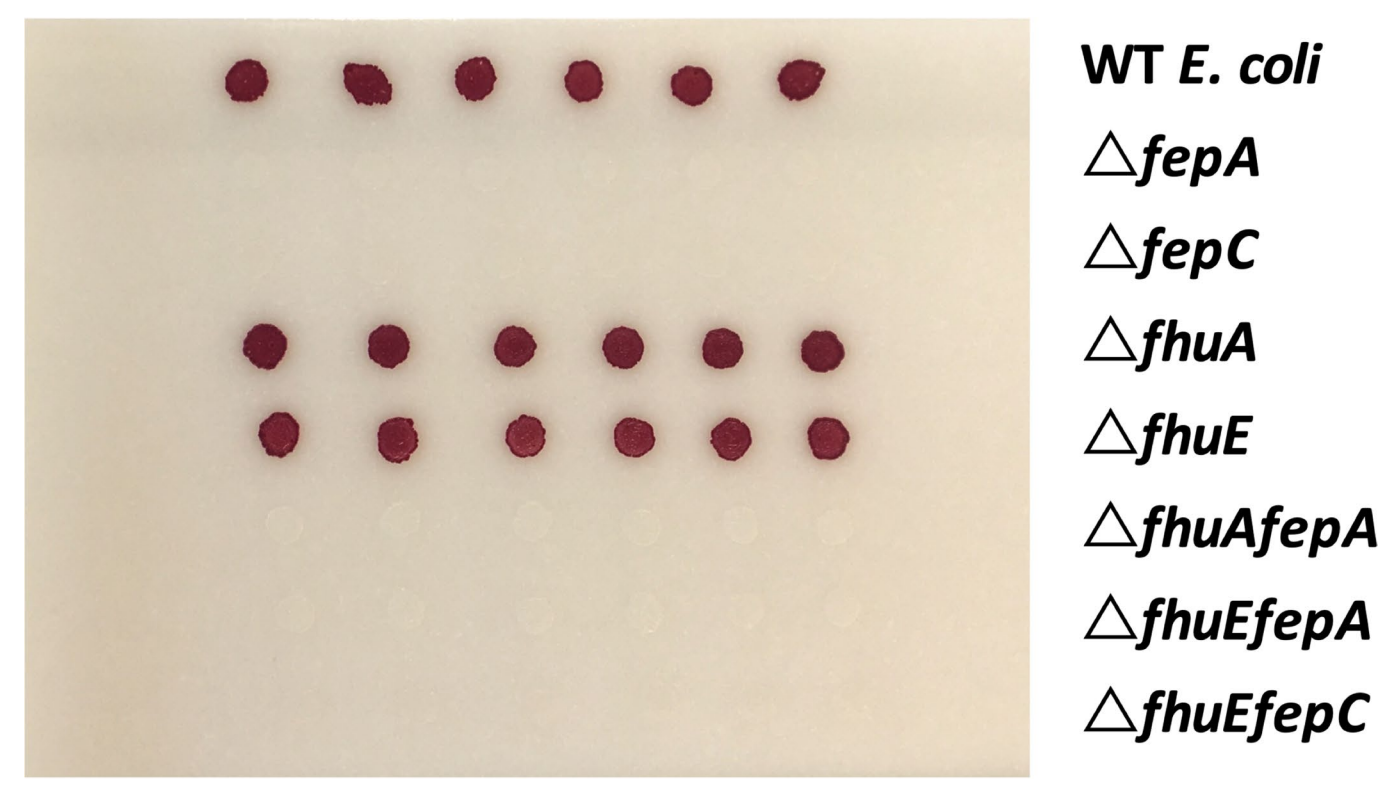
**Extended Data Fig. 6 | Clusters of Orthologous Genes (COG) categories of genes with interaction fitness.** Charts display the number of genes with interaction fitness that fall into each COG category for *E. coli* (left) or *P. psychrophila* (right).



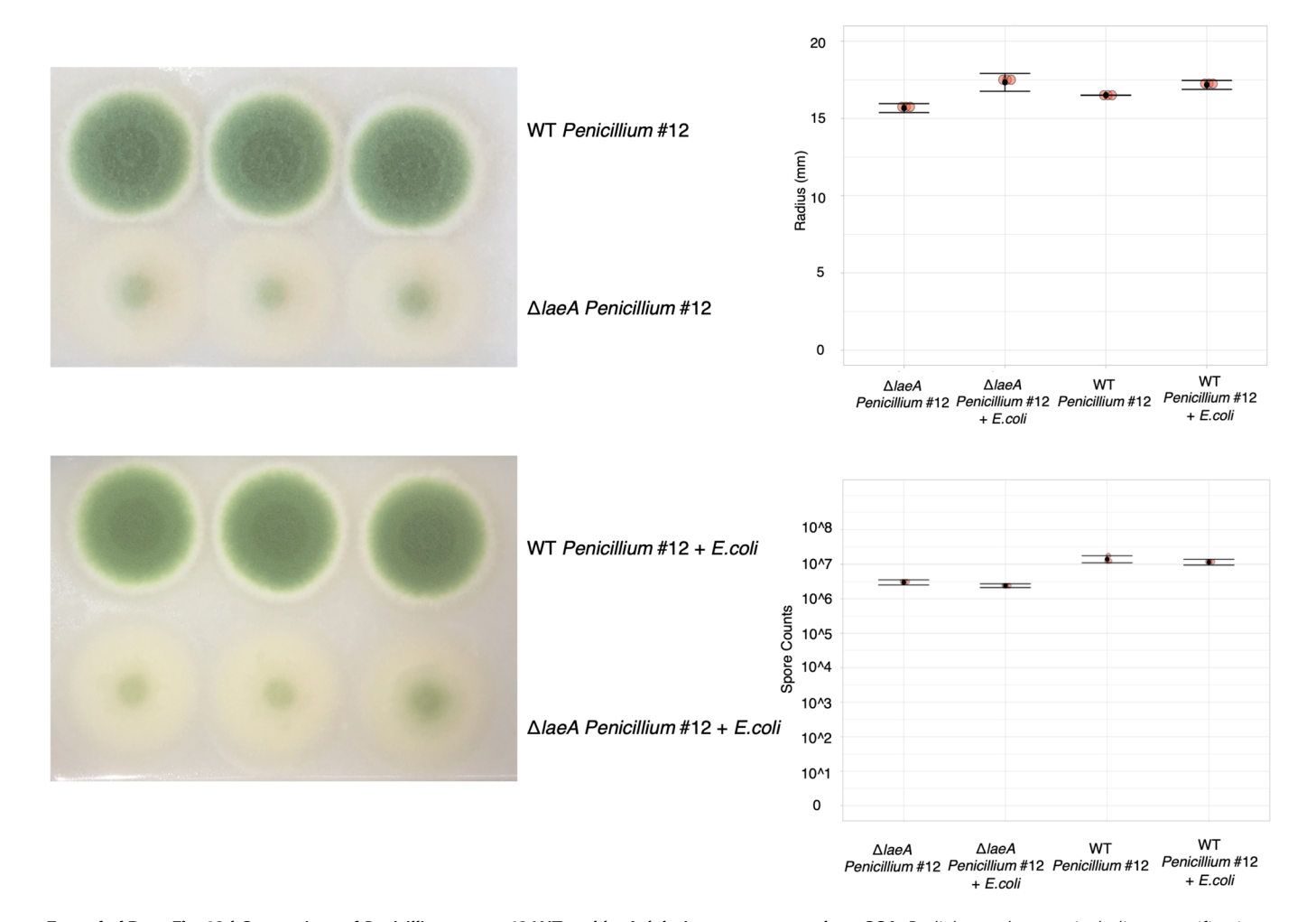
Extended Data Fig. 7 | Bacterial Cytological Profiling of  $\Delta$ tolC E.coli treated with known antibiotic compounds on cheese curd agar. DAPI dye stains DNA and FM4-64 dye stains bacterial membranes. SYTOX green stains nucleic acids but cannot penetrate live cells. Scale bars represent 2  $\mu$ m. Testing of each antibiotic at four concentrations was performed once, and cells from the edges of zones of clearing were imaged for at least 5 fields from each condition to ensure consistency in phenotype.



**Extended Data Fig. 8 | Siderophore production by filamentous fungi.** Liquid CAS assay was performed on filtered and concentrated fungal supernatants from three replicates grown in 2% liquid cheese pH 7 for 12 days. Row A) 1-3: Liquid cheese control 4-6: *Penicillium* SAM3. Row B) 1-3: *Debaryomyces* 135B 4-6: *Penicillium* #12. Row C) 1-3: *Candida* 135E. 4-6: *Penicillium* RS17. Row D) 1-3: *Scopulariopsis* 165-5 Row E) 1-3: *Scopulariopsis* JB370. Row F) 1-3: *Fusarium* 554A. % Siderophore units calculated as  $[(A_r - A_s)/(A_r)]^*100$ , where A<sub>r</sub> is the absorbance of the cheese curd agar supernatant blank and A<sub>s</sub> is the absorbance of the sample. N=3 biologically independent samples, error bars show standard deviation and black point is the mean.



**Extended Data Fig. 9 | Fitness defect of \Delta** fee mutants on iron-limiting CCA. Visual assays of *E. coli* mutant growth spotted alone on CCA pH 7 supplemented with tetrazolium chloride, an indicator of respiration.



**Extended Data Fig. 10 | Comparison of** *Penicillium* **sp. str. 12 WT and** *laeA* **deletion mutant growth on CCA.** Radial growth assay, including quantification, of *Penicillium* sp. str. 12 WT and *laeA* deletion mutant grown alone or with *E. coli* on CCA pH 7 (N=3 biologically independent experiments, error bars show standard deviation and black point is the mean). Spore counts from *Penicillium* sp. str. 12 WT and *laeA* deletion mutant grown alone or with *E. coli* for 7 days on CCA are also shown (N=3 biologically independent samples, error bars show standard deviation and black point is the mean).



Corresponding author(s):	Rachel Dutton
Last updated by author(s):	Aug 19, 2020

# Reporting Summary

Nature Research wishes to improve the reproducibility of the work that we publish. This form provides structure for consistency and transparency in reporting. For further information on Nature Research policies, see Authors & Referees and the Editorial Policy Checklist.

_					
۷ŧ	1	t١	ςt	10	c
- N I	_		<b>ST</b>	ш	-

FUI	dii Si	adistical analyses, commit that the following items are present in the righter legend, table regend, main text, or Methods section.
n/a	Coi	nfirmed
		The exact sample size (n) for each experimental group/condition, given as a discrete number and unit of measurement
		A statement on whether measurements were taken from distinct samples or whether the same sample was measured repeatedly
		The statistical test(s) used AND whether they are one- or two-sided  Only common tests should be described solely by name; describe more complex techniques in the Methods section.
X		A description of all covariates tested
		A description of any assumptions or corrections, such as tests of normality and adjustment for multiple comparisons
		A full description of the statistical parameters including central tendency (e.g. means) or other basic estimates (e.g. regression coefficient) AND variation (e.g. standard deviation) or associated estimates of uncertainty (e.g. confidence intervals)
		For null hypothesis testing, the test statistic (e.g. $F$ , $t$ , $r$ ) with confidence intervals, effect sizes, degrees of freedom and $P$ value noted Give $P$ values as exact values whenever suitable.
	$\boxtimes$	For Bayesian analysis, information on the choice of priors and Markov chain Monte Carlo settings
$\times$		For hierarchical and complex designs, identification of the appropriate level for tests and full reporting of outcomes
	$ \boxtimes$	Estimates of effect sizes (e.g. Cohen's $d$ , Pearson's $r$ ), indicating how they were calculated

Our web collection on <u>statistics for biologists</u> contains articles on many of the points above.

# Software and code

Policy information about availability of computer code

Data collection

Deltavision SoftWorx software 5.5.1 was used for collection of microscopy images (Figure 4, Supplementary Figure 9).

Data analysis

The custom R scripts developed for processing RB-TnSeq data described in this manuscript are available at https://github.com/ DuttonLab/RB-TnSeq-Microbial-interactions along with usage instructions. The perl scripts used for initial processing of RB-TnSeq data published in Wetmore et al. 2015 are available at https://bitbucket.org/berkeleylab/feba/src/master/. Geneious version R9 9.1.8 was used for ribosomal subunit sequence alignment and the MrBayes plugin was used for creation of the phylogenetic tree in Figure 1; FigTree v1.4.4 was used for visualization. Global Natural Products Social Molecular Networking (GNPS), including the Dereplicator+ tool, was used to analyze mass spectrometry data and is available at https://gnps.ucsd.edu/ProteoSAFe/static/gnps-splash.jsp. XCMS Online version 2.7.2 (https://xcmsonline.scripps.edu/landing\_page.php?pgcontent=mainPage) was used to make the cloud plot in Figure 6d. ClusterProfiler (R package version 3.12.0) was used for GO ontology functional enrichment analysis of bacterial gene sets. For P. psychrophila, a custom annotation database was created for use in ClusterProfiler using AnnotationForge (R package version 1.26.0). Cytoscape v. 3.5.1 was used to create the networks seen in Figures 3 and 5. R package ggfortify 0.4.7 was used to make PCA plots. R package UpSetR v. 1.4.0 was used to make UpSet plots. COG category mapping was done with eggNOG-mapper v2. Microscopy images in Figure 4 were deconvoluted using Deltavision SoftWorx 5.5.1 software, analyzed using Fiji ImageJ 1.52h, and assembled in Adobe Photoshop CC 2018. The following tools were used for RNA-Seq analysis: Geneious version R9 9.1.8, Rsamtools (R package version 2.0.3), GenomeInfoDb (R package version 1.20.0), GenomicFeatures (R package version 1.36.4), GenomicAlignments (R package version 1.20.1), GenomicRanges (R package version 1.36.1), DESeq2 (R package version 1.20.1), and KOBAS 3.0. Plots in Figures 2, 3, 5, and 6, Supplementary Figures 1, 2, and Extended Data 3, 5, 8, and 10 were made with R package ggplot 23.2.1. AntiSMASH 5.0 was used for secondary metabolite biosynthesis cluster prediction. For Oxford Nanopore sequencing data, data was basecalled using guppy 3.3.0, assembled with canu 1.8, and polished with racon 1.4.3 and pilon 1.23.

For manuscripts utilizing custom algorithms or software that are central to the research but not yet described in published literature, software must be made available to editors/reviewers. We strongly encourage code deposition in a community repository (e.g. GitHub). See the Nature Research guidelines for submitting code & software for further information.

# Data

Policy information about availability of data

Clinical data

All manuscripts must include a data availability statement. This statement should provide the following information, where applicable:

- Accession codes, unique identifiers, or web links for publicly available datasets
- A list of figures that have associated raw data
- A description of any restrictions on data availability

Sequence data that support the findings of this study (RB-TnSeq, RNA-Seq) have been deposited in the NCBI SRA database with SRA accession codes SRR11514793-SRR11514872 and BioProject PRJNA624168. Mass spectrometry data is available in the MassIVE database under accession numbers MSV000085070 and MSV000085054. The GNPS molecular network is available at https://gnps.ucsd.edu/ProteoSAFe/status.jsp?task=464b331ef9d54de9957d23b4f9b9db14. The E. coli annotation database used for gene ontology functional enrichment is available at http://bioconductor.org/packages/release/data/annotation/html/ org.EcK12.eg.db.html. The Whole Genome Shotgun project for Penicillium sp. str. #12 including reads, genome assembly, and annotation has been deposited at DDBJ/ENA/GenBank under the accession JAASRZ000000000 in BioProject PRJNA612335 (BioSample SAMN14369290 and SRA SRR11536435). In addition to these sources, data used to create figures 2,3,5, and 6 is available in the Supplementary Tables provided with the paper.

Field-spe	ecific reporting		
Please select the o	ne below that is the best fit for	your research. If you are not sure, read the appropriate sections before making your selection.	
Life sciences	Behavioural & so	cial sciences	
For a reference copy of	the document with all sections, see <u>natu</u>	re.com/documents/nr-reporting-summary-flat.pdf	
Life scier	nces study des	ign	
	sclose on these points even who		
Sample size	This study uses clonal bacterial strains that are highly reproducible. We used at least 3 biological replicates for all experiments as it is standard practice for most microbiological assays. No sample size calculation was performed to determine sample size.		
Data exclusions	No data were excluded from the analyses.		
Replication	All competitive growth experiments, RB-TnSeq assays, RNA-Seq assays, CAS assays, biotin quantification, and mass spectrometry data collections were performed at least in triplicate from distinct samples. All attempts at replication were successful. For RB-TnSeq assays, the mutant library has a median of 16 (E. coli) or 18 (P. psychrophila) insertion mutants per gene, which can also be treated as replicates within each biological sample.		
Randomization	Randomization is not relevant to and was not performed in this study. No group allocation occurred.		
Blinding	Blinding is not relevant to and wa	s not performed in this study. No group allocation occurred.	
<u> </u>	<u> </u>	naterials, systems and methods of materials, experimental systems and methods used in many studies. Here, indicate whether each material.	
'	/ 1	are not sure if a list item applies to your research, read the appropriate section before selecting a response.	
Materials & experimental systems Meth		Methods	
n/a Involved in the study		n/a Involved in the study	
Antibodies		ChIP-seq	
Eukaryotic cell lines		Flow cytometry	
Palaeontology		MRI-based neuroimaging	
	Animals and other organisms  Human research participants		
ZIII Hamaines			